

Clustering at High Redshift: Precise Constraints from a Deep, Wide Area Survey

Marc Postman¹

Space Telescope Science Institute², Baltimore, MD 21218

Tod R. Lauer

National Optical Astronomy Observatories³, Tucson, AZ 85726

István Szapudi

University of Durham, Department of Physics, South Road, Durham, DH1 3LE, UK

William Oegerle¹

Johns Hopkins University, Department of Physics & Astronomy, Baltimore, MD 21218

Accepted for publication in the *Astrophysical Journal*

arXiv:astro-ph/9804141v2 12 May 1998

¹Visiting Astronomer Kitt Peak National Observatory, NOAO.

²The Space Telescope Science Institute is operated by the Association of Universities for Research in Astronomy (AURA), Inc., under National Aeronautics and Space Administration (NASA) Contract NAS 5-26555.

³The National Optical Astronomy Observatories are operated by AURA, Inc., under cooperative agreement with the National Science Foundation.

ABSTRACT

We present constraints on the evolution of large-scale structure from a catalog of 710,000 galaxies with $I_{AB} \leq 24$ derived from a KPNO 4m CCD imaging survey of a contiguous $4^\circ \times 4^\circ$ region. The advantage of using large contiguous surveys for measuring clustering properties on even modest angular scales is substantial: the effects of cosmic scatter are strongly suppressed. We provide highly accurate measurements of the two-point angular correlation function, $\omega(\theta)$, as a function of magnitude on scales up to 1.5° . The amplitude of $\omega(\theta)$ declines by a factor of ~ 10 over the range $16 \leq I \leq 20$ but only by a factor of $2 - 3$ over the range $20 < I \leq 23$. For a redshift dependence of the spatial correlation function, $\xi(r)$, parameterized as $\xi(r, z) = (\frac{r}{r_o})^{-\gamma}(1+z)^{-(3+\epsilon)}$, we find $r_o = 5.2 \pm 0.4h^{-1}$ Mpc, and $\epsilon \gtrsim 0$ for $I \leq 20$. This is in good agreement with the results from local redshift surveys. At $I > 20$, our best fit values shift towards lower r_o and more negative ϵ . A strong covariance between r_o and ϵ prevent us from rejecting $\epsilon > 0$ even at faint magnitudes but if $\epsilon > 1$, we strongly reject $r_o \lesssim 4h^{-1}$ Mpc (co-moving). The above expression for $\xi(r, z)$ and our data give a correlation length of $r_o(z = 0.5) \approx 3.0 \pm 0.4h^{-1}$ Mpc, about a factor of 2 larger than the correlation length at $z = 0.5$ derived from the Canada–France Redshift Survey (CFRS; Le Fevre *et al.* (1996)). The small volume sampled by the CFRS and other deep redshift probes, however, make these spatial surveys strongly susceptible to cosmic scatter and will tend to bias their derived correlation lengths low. Our results are consistent with redshift distributions in which $\sim 30 - 50\%$ of the galaxies at $I = 23$ lie at $z > 1$. The best fit power law slope of the correlation function remains independent of I magnitude for $I \leq 22$. At fainter limits, there is a suggestive trend towards flatter slopes that occurs at fluxes consistent with similar trends seen by Neuschaffer & Windhorst (1995) and Campos *et al.* (1995). The galaxy counts span 11 magnitudes and provide an accurate calibration of the galaxy surface density. We find evidence for mild galaxy evolution – about 1 mag of brightening or a doubling of the density by $I = 23$ relative to an $\Omega_o = 1$ no evolution model; about 0.5 mag of brightening or a factor of 1.5 increase in surface density relative to an open model. Our galaxy counts agree well with those from the HDF survey and, thus, argue against a significant inclusion of sub-galactic components in the latter census for $I < 24$.

Subject headings: large-scale structure, clustering, galaxy evolution, galaxy catalogs

1. Introduction

The evolution of large-scale structure (LSS) in the universe probes the abundance and form of dark matter, the mean baryon density, the turnover scale in the perturbation power spectrum, and the formation processes of galaxies and clusters. Observational constraints on the evolution of LSS provide strong limits on structure formation theories because the sensitivity of the mass function to Ω_o is high and because coherent structures on scales $> 10h^{-1}$ Mpc are still in the linear regime, precisely where important distinctions can be made between competing theories. A study of this evolution is, thus, fundamental. Substantial progress has been made in studying LSS evolution from deep redshift surveys. The general consensus from the most distant probes (Cohen *et al.* (1996), Steidel *et al.* (1998), Giavalisco *et al.* (1997)) suggests that there has been significant evolution in the clustering properties of galaxies since $z \sim 3$. Precisely just how much

evolution has occurred since $z \sim 1$ is less certain but the data are being accumulated rapidly (Lilly *et al.* (1995), Le Fevre *et al.* (1995), Connolly *et al.* (1996), Connolly, Szalay, & Brunner (1998)).

Two-dimensional surveys offer some key advantages over narrow, deep redshift surveys like those above. Specifically, a large area angular survey subtends many galaxy correlation lengths in the transverse direction enabling many independent cells to contribute to the signal at a given depth. In addition, the power spectra derived from angular surveys are unaffected by redshift distortions, which tend to wash out small-scale power. The disadvantage of a 2D survey, of course, is that the depth sampled in a given flux range is usually broad and one must therefore deal with projection effects. Observationally, mapping large areas of sky is now quite an efficient process due to the availability of large-format CCD arrays and mosaic cameras. Ideally, one would like to conduct deep redshift surveys that also cover large, quasi-contiguous areas. As an initial step towards this goal, we have surveyed a contiguous 16 square degree area in the I -band using the prime focus CCD camera on the Mayall 4m at Kitt Peak National Observatory. The area is about an order of magnitude larger than any comparably deep, contiguous survey yet published. Our goal is to set accurate limits at $z = 1$ on the amplitude of structures now seen at $z = 0$.

The study of large-scale structure has advanced primarily through the study of the moments of the galaxy distribution. These fundamental functions, which must be explained by any viable structure formation model, are determined, in part, by the initial conditions at recombination and by subsequent non-linear growth. The presence of non-zero high order moments ($n \geq 3$) provide constraints on the non-Gaussian properties of the galaxy distribution and, hence, provide very strong discrimination between competing models. The first two moments, however, are essential for assessing departures from a non-evolving, Poisson distribution. The combination of area and depth provided by this survey ($\sim 710,000$ galaxies with $I_{AB} \leq 24$) allows us to determine the first two moments with significantly lower uncertainties than previous works. For example, the angular two-point correlation function at faint magnitudes has been measured on scales of $\lesssim 10$ arcminutes (*e.g.*, Efstathiou *et al.* (1991), Neuschaffer & Windhorst (1995), Campos *et al.* (1995), Lidman & Peterson (1996), Woods & Fahlman (1997), Brainerd & Smail (1997)) but there is substantial scatter in the results at $I \gtrsim 21$, which has led to conflicting conclusions about the evolution of structure. A significant reason for the scatter is the relatively small ($\lesssim 0.25 \text{ deg}^2$) contiguous areas used. At these scales, one is subject to both cosmic variations in clustering and systematic corrections that are comparable in amplitude with the signal being measured. Such effects are negligible for the present survey and thus enable a major enhancement to the precision and accuracy of LSS and evolution measurements. Furthermore, the survey supports a reliable determination of at least the 3rd and 4th moments of the galaxy distribution.

In this paper we present the I -band galaxy counts and constraints on the evolution of the two-point correlation function. An analysis of the higher moments ($n = 3, 4$) of the galaxy distribution will be presented in a separate paper (Szapudi *et al.* (1998)). Section 2 contains a brief description of the observations and survey strategy. Section 3 presents results for the I -band galaxy counts. Our results for the two-point angular correlation function are presented in Section 4. The interpretation of our results is discussed in Section 5. We adopt $h = H_0/(100 \text{ km sec}^{-1} \text{ Mpc}^{-1})$.

2. Survey Strategy and Observations

The primary goal of the survey is to use distant clusters of galaxies to explore LSS out to $z = 1$. To do this reliably, the survey had to subtend at least $\sim 75h^{-1}$ Mpc in at least one of the angular directions given

that the local correlation length of clusters is $15 - 20h^{-1}$ Mpc (Postman *et al.* (1992), Dalton *et al.* (1994), Croft *et al.* (1997)). At $z = 1$, $75h^{-1}$ Mpc subtends 4.1° for $q_o = 0.1$ (4.9° for $q_o = 0.5$). Furthermore, to measure the high redshift cluster correlation function with accuracies approaching those of low redshift studies, the survey needed to contain at least 150 – 200 clusters with $z \geq 0.3$. Estimates of the surface density of clusters (Gunn *et al.* (1986), Postman *et al.* (1996)) are in the range 10 – 15 clusters/deg² out to $z = 1$, thus an area of at least 15 square degrees was needed. Additional survey size constraints were imposed by the desire to accurately measure the galaxy angular two-point correlation function, $\omega(\theta)$, on scales up to $\sim 1^\circ$ at faint magnitudes. This required that the survey subtend at least 3° to minimize the effects of the integral constraint on $\omega(\theta)$ on scales $\theta < 1^\circ$. These requirements, plus the desire to avoid severe aliasing effects and unfavorable window functions, led us to choose a $4^\circ \times 4^\circ$ survey geometry.

The KPNO 4m prime focus CCD camera has a $16'$ field of view (0.47 arcseconds per pixel); 256 exposures were, therefore, required to survey the entire field. Each pointing overlapped its adjacent pointing by 1 arcminute. Local stability of the zeropoint is provided by comparing the overlap regions of any given CCD field with its neighbors. By comparing the photometry of objects in common in any overlap region, we find that we can measure the relative photometric offsets between any two images to 0.03 mag. We then solve for relative offsets of all images in the survey by a system of linear equations that minimizes the local differences between the images and their neighbors. Simulations of this operation show that the local error in the zeropoint of any image is ~ 0.016 mag which translates to a limit on the random error in $\omega(\theta)$ of $\lesssim 0.001$ due to frame-to-frame zeropoint variations. As roughly half of the images were obtained in non-photometric conditions, this allows us to still calibrate the survey from the photometric set of images. Unfortunately, building the calibration from a set of local differences is poor at preserving a constant zeropoint over large scales. To provide for stability of the zeropoint over the extent of the survey, we used large-area calibration frames obtained under photometric conditions at the KPNO 0.9m telescope by Ralph Shuppig. The calibration frames were interspersed throughout the survey area, and provide a check against large-scale gradients in the calibration. Based on the quality of this material, we estimate that the zeropoint is constant over both 4° dimensions of the survey to $\lesssim 0.04$ mag which translates to a systematic error in $\omega(\theta)$ $\lesssim 0.003$ on a 4° scale and proportionally less on smaller scales. Indeed, computation of $\omega(\theta)$ in the independent quadrants of the survey yields results which are consistent with one another at the above level.

We selected the field centered at 10h 13m 27.95s +52d 36m 43.5s (J2000) by virtue of its high galactic latitude ($+51^\circ$), low HI column density ($2.2 \times 10^{20} \text{ cm}^{-2}$), high declination (extended visibility from KPNO), low IRAS 100μ cirrus emission, and the absence of many bright stars or nearby rich clusters. In a survey of this size, however, it is impossible to avoid all bright ($I \leq 16$) stars. The effective area of the survey is 14.7 deg² after we exclude those pixels in the vicinity of these bright objects.

Each exposure was 900 seconds in duration yielding images with a 5σ limit at $I_{AB} = 24$ and sufficient depth to detect cluster galaxies 2 magnitudes fainter than the typical unevolved first-ranked elliptical at $z = 1$. This depth was essential — a shallower survey would only be sufficient for detecting the very richest $z \sim 1$ clusters (at $I_{AB} = 24$, we are able to detect $z \sim 1$ Abell richness class 1 systems) and would limit visibility of structure evolution.

3. Galaxy Counts

Automated object detection and classification were performed using a modified version of the FOCAS package (Valdes (1982)). Modifications include the use of a position-dependent point spread function (PSF), an essential feature for accurate star/galaxy classification in data obtained with the KPNO PFCCD system. Extensive catalog quality assurance was performed to verify object classification accuracy and to remove spurious detections near bright objects. A detailed description of the galaxy catalog construction process is discussed in Postman *et al.* (1998). However, it is important to provide a brief description of the star-galaxy classification procedure here. The object classification is done on a frame-by-frame basis. First, the PSF in each image is determined using a set of compact, symmetric objects (this is accomplished with the FOCAS *autopsf* routine). To assure the code has not selected inappropriate objects, each derived PSF is visually inspected and a quick comparison is made with the actual image frame to assess whether the PSF template is sensible. In about 10 – 15% of the cases, stellar templates had to be selected manually. Second, a polynomial representation of the PSF variation as a function of distance, r , from the camera’s optical center is made. (Specifically, we find the function $B(r) = a_0 + a_2r^2 + a_4r^4$ is an accurate model of the variation in the KPNO camera prior to the installation of the new prime focus corrector/ADC in June 1997). The optical center is determined directly from the data by mapping the stellar surface density (using a position-independent PSF classifier) as a function of CCD position. Failure to use a position-dependent PSF results in a paucity of stars near the CCD edges which traces the optical distortions. Finally, each detected object is classified as a star or galaxy based on fitting both an unbroadened and broadened PSF to the two-dimensional object image. Any object which requires a component broader than 1.3 times the nominal PSF *at the object’s position on the frame* is considered to be a galaxy. The stellar surface density derived from position-dependent PSF classification shows no variation with distance from the optical center. This classification method works well down to about $I=21.5$ in these data (based on running the same code on simulations). Fainter than this, a statistical approach is needed to assess the probability that an object is a galaxy. However, for $I > 21.5$ galaxies outnumber stars by at least a factor of 5 (the galaxy/star ratio is ~ 10 by $I = 23.5$, based on an extrapolation of the star and galaxy counts measured to $I = 21.5$). Hence, star contamination would not exceed $\sim 10 - 15\%$ even if one simply classified every object fainter than $I = 21.5$ as a galaxy. We, however, do use a probability derived from the extrapolated galaxy/star ratio to classify objects fainter than $I = 21.5$.

Figure 1 and Table 1 show the differential number of galaxies per unit area per magnitude as a function of I magnitude. Also shown in Figure 1 are the predictions from the dwarf-dominated, no-evolution models of Ferguson & Babul (1998) and the counts from the Hubble Deep Field (Williams *et al.* (1996)) all adjusted to the Cousins I system. The curvature seen in the I -band log N-mag relationship is real – the effects of object misclassification and incompleteness are negligible for $I \leq 21$ and have been accurately modeled and removed at fainter magnitudes as discussed above. The slope of the relationship monotonically decreases in a nearly linear fashion from the Euclidean value of 0.60 at $I = 15$ to 0.27 by $I = 23.5$. Figure 2 demonstrates how our counts compare with previous determinations. For clarity, we have normalized all results by $\text{dex}(0.6(I - 18))$. Our counts are in good agreement with those of Lilly *et al.* (1991), Smail *et al.* (1995), Le Fevre *et al.* (1995) (CFRS), Williams *et al.* (1996), and Gardner *et al.* (1996). Our survey provides a homogeneous calibration of the I -band galaxy counts over an 11 magnitude range ($13 \leq I \leq 24$), and actually covers more area at the *bright* end ($I < 19$) than any of these earlier surveys. This is an important step towards removing ambiguities in the galaxy number counts at brighter magnitudes. We find that the CFRS counts are systematically high for $I < 19$ and the Hubble Deep Field (HDF) counts are systematically high for $I < 21$. However, the errors for those surveys are

large in those intervals owing to their small angular coverage and the difference is entirely consistent with the observed cosmic fluctuations in counts on scales of a few arcminutes and probable small differences in isophotal detection limits. Our agreement with the HDF counts in the range $21.7 \lesssim I \lesssim 24$ is quite important because it suggests that both the HDF galaxy catalog and ours appear to be counting the same type of objects at least in this magnitude range. Given HST’s superior resolution, this would argue that down to $I = 24$ inclusion of a significant population of sub-galactic clumps in the HDF counts is not likely (Colley *et al.* (1996)).

We have normalized the no-evolution models to match our counts precisely at $I \leq 16$ where the models and the data exhibit the same near-Euclidean slope of 0.55. This is the most appropriate normalization location since we want to test for departures from the no-evolution assumption at cosmological distances. Relative to the no-evolution $\Omega = 1$ model at $I = 23$ ($0.7 \lesssim z_{\text{median}} \lesssim 1$), our counts are consistent with either ~ 1 mag of luminosity evolution or a factor of ~ 2 enhancement in the galaxy density. Relative to the $\Omega = 0.02$ model at this same magnitude, our counts are consistent with either ~ 0.5 mag of luminosity evolution or a factor of ~ 1.5 enhancement in the galaxy density. While these models fail to reproduce the very faint Hubble Deep Field observations (see Ferguson & Babul (1998)), they do reasonably well at brighter magnitudes and thus provide a plausible comparison in the flux regime covered by our survey.

4. The Two-point Correlation Function

We use the Landy & Szalay (1993) estimator, $\omega(\theta) = (DD - 2DR + RR)/RR$, to compute the two-point angular correlation function. Here DD is the observed number of galaxy pairs with separation between θ and $\theta + \delta\theta$, RR is the number of such pairs in a randomly distributed sample with identical boundaries and galaxy surface density, and DR is the number of such pairs in a cross-correlation between the observed catalog and a random realization. This is the minimum variance estimator and fully corrects for mask and edge effects up to scales approaching the survey size. Our results for 9 independent magnitude slices, each based on 100 random realizations, are shown in Figure 3 after the application of the integral constraint (IC) and stellar contamination corrections. The IC correction attempts to offset the artificial reduction in power on large scales that occurs when the mean galaxy density and $\omega(\theta)$ are determined from the same survey (Groth & Peebles (1977)). The small reduction in amplitude introduced by misclassified stars is corrected by multiplying the IC-corrected $\omega(\theta)$ values by the factor $N_{Obj}^2 / (N_{Obj} - N_{Star})^2$ where N_{Obj} is the total number of objects in a given magnitude bin and N_{Star} is an estimate of the number of misclassified stars in the same bin. Since galaxies significantly outnumber stars when $I > 21.5$, stellar contamination effects are most significant for brighter magnitudes. However, that is precisely where the PSF-based classifier works extremely well. Hence we take the number of misclassified stars to be approximately equal to the square root of the number of stars in the bin. We have confirmed that the results from Landy-Szalay estimator are in excellent agreement with those from alternative estimators for $\omega(\theta)$ such as the counts-in-cells method or the ensemble estimator. In each magnitude slice, we only include data from those CCD images in the survey that are complete to at least 0.5 mag fainter than the upper mag limit of the slice. This assures that large-scale artificial power from frame-to-frame depth variations is eliminated. The depth of each frame is determined by identifying the location of the peak object counts (stars plus galaxies) and then subtracting 0.25 mag.

We find excellent agreement between our results for $17 \leq I < 18.25$ and the APM $\omega(\theta)$ determination (Maddox *et al.* (1996)) derived from galaxies with $17 \leq b_J \leq 20$ (dashed line). Table 2 presents our correlation function data (multiplied by 100 for compactness) in each magnitude bin. The data in this table

have the IC and stellar contamination corrections applied. Table 3 presents the median I magnitudes, number of galaxies each subsample, best fit power law slopes, the corrected amplitudes at 0.5, 1, and 3 arcminutes (interpolated from results in Table 2), and the values of the IC and stellar contamination corrections. The slope of the correlation function is determined from the best fit to the power law representation $\omega(\theta) = A_\omega \theta^\delta$. The formal error in $\omega(\theta)$ is $\sigma_\omega = \sqrt{(1 + \omega(\theta))/\text{RR}}$. This expression produces error values which are comparable to those estimated by the statistical bootstrap method. The errorbars in Figure 3 (and Table 2) include an often ignored additional error term, added in quadrature to the formal error, arising from uncertainty in the value of the IC. The IC uncertainty arises because one typically assumes a power-law form for $\omega(\theta)$ a priori and thus, on large scales, systematic errors can be introduced if this is not an accurate representation of the true correlation function. We estimate this uncertainty by measuring the change in the IC as the assumed power law slope is varied by ± 0.1 . Strictly, these two error components are not completely independent (and thus a quadrature addition is not completely proper). However, the quadrature addition provides a reasonable approximation and, for the present survey, the IC uncertainty is only important (*i.e.*, becomes comparable to the formal error above) on scales $\theta \gtrsim 25$ arcminutes.

4.1. Dependence of the Amplitude on Magnitude

Figure 4 shows the dependence of the amplitude of $\omega(\theta)$ at $1'$ scale on the median I magnitude of the subsample. Results from Efstathiou *et al.* (1991), Campos *et al.* (1995), Neuschaffer & Windhorst (1995), Lidman & Peterson (1996), Woods & Fahlman (1997), and Brainerd & Smail (1997) are shown for comparison. We find a smooth decline in amplitude with median I magnitude that is consistent with the results from Campos *et al.* (1995) and Brainerd & Smail (1997). For $I \lesssim 21$, our results are also consistent with those of Lidman & Peterson (1996), although their results are systematically lower in amplitude by 20% to 45%. At $I > 22$, we differ at more than the 3σ level from the results of Lidman & Peterson (1996) and Woods & Fahlman (1997).

Our results are substantially more reliable than previous estimates over the range $I < 24$ because our large survey area overcomes the most significant problem faced by smaller surveys: the cosmic variance in galaxy surface density and clustering. For small surveys, these effects result in large fluctuations in the correlation amplitude and in a large value of the IC correction on arcminute scales. At large scales both of these effects depend on the average of the correlation function over the survey area. The ratio of variances expected between two different surveys is at least $(\theta_1/\theta_2)^{\delta/2}$, where θ_1 and θ_2 are the effective angular scales of the two surveys and δ is the slope of the angular correlation function. While cosmic variance is boosted at small scales by the higher order correlations neglected in this simplified formula, the formula should be a reasonable accurate approximation for the ratio of finite volume errors. Thus, relative to many of the previous surveys, the cosmic variance on arcminute scales in our survey is suppressed by more than a factor of 3. Moreover, the continuity and simple geometry of our survey together with the large number of galaxies employed ensure that edge and discreteness effects are negligible over a large dynamic range of scales. The advantage of this large, contiguous area surveys is, therefore, even better than the above estimate.

In addition to the above effects, which primarily depend on the variance only, the non-Gaussian error distribution for $\omega(\theta)$ is likely to be skewed positively (Szapudi & Colombi (1996)) as well. This can result in an *apparent* low bias in the correlation amplitude for smaller surveys since there are many areas of sky with values somewhat lower than the mean, which are not balanced by the relatively few areas with values much higher than the mean. We use our survey data to directly measure the true variance caused by

surface density and clustering properties in $\omega(1')$ in many independent but small contiguous areas, and find that variance is significant on 1 arcminute scales. We chose a cell size of $16' \times 16'$ — corresponding to the field of view of a single KPNO 4m CCD exposure (which is still significantly larger than the independent fields of previous surveys). We analyze 250 such fields and computed $\omega(\theta)$ for $21 \leq I \leq 22$, a magnitude range where we begin to see growing discrepancy between different surveys. The histogram of $\omega(1')$ values is shown in Figure 5. We find that the scatter in $\omega(1')$ is comparable to its mean value (~ 0.045). Extreme values can reach $3\times$ the mean. Thus, in order to measure $\omega(1')$ with a S/N of 10 one requires at least 100 such independent fields even at only moderately faint magnitudes. There is also a 20% offset between the full survey value and the mean of the 250 independent fields, but this difference is entirely consistent with uncertainties in the IC correction for the individual CCD frame results.

The IC correction, like cosmic variance, is determined by the effective survey area, and to lesser extent, by the survey geometry. The largest contiguous area used in $\omega(\theta)$ measurements at $I \geq 22$ in the other works cited is 0.25 deg^2 (compared with 14.7 deg^2 here). The IC corrections at $1'$ in our survey are negligible ($\lesssim 0.05\omega(\theta)$) whereas they can be a significant fraction ($\sim 50 - 100\%$) of the amplitude of $\omega(\theta)$ in some of the previous surveys (*e.g.*, Efstathiou *et al.* (1991)). Hence, while the agreement between Brainerd & Smail (1997) and our results is excellent, their two survey fields only cover about 0.02 deg^2 and, therefore, additional imaging over larger areas at fainter limits ($I > 24$) is still desired. The Campos *et al.* (1995) results are based on a survey of $64 \ 11' \times 11'$ non-contiguous fields (2.2 deg^2 total area) distributed over an $8^\circ \times 10^\circ$ region.

4.1.1. Models

The dependence of the angular correlation function amplitude on magnitude can be modeled using the equation (Limber (1953), Peebles (1980))

$$\omega(\theta) = \sqrt{\pi} \frac{\Gamma[(\gamma - 1)/2]}{\Gamma(\gamma/2)} \frac{A(\epsilon)}{\theta^{\gamma-1}} r_o^\gamma \quad (1)$$

that relates $\omega(\theta)$ to the spatial correlation function, $\xi(r) = (r/r_o)^{-\gamma}$. A power-law spatial correlation function implies that its two dimensional counterpart, $\omega(\theta)$, will also take on a power-law form. The function $A(\epsilon)$ depends on the galaxy redshift distribution, $N(z)$, and on the evolution of $\xi(r)$. If this evolution is parameterized as (*e.g.*, Efstathiou *et al.* (1991) and Woods & Fahlman (1997))

$$\xi(r, z) = \left(\frac{r}{r_o}\right)^{-\gamma} (1+z)^{-(3+\epsilon)} \quad (2)$$

then $A(\epsilon)$ is

$$A(\epsilon) = \int_0^\infty D(z)^{1-\gamma} g(z)^{-1} (1+z)^{-(3+\epsilon)} \left(\frac{dN(z)}{dz}\right)^2 dz \left[\int_0^\infty \left(\frac{dN(z)}{dz}\right) dz \right]^{-2} \quad (3)$$

where $D(z)$, the angular diameter distance, and $g(z)^{-1}$ are

$$D(z) = \frac{c}{H_o} \left(\frac{q_o z + (q_o - 1)(\sqrt{1 + 2q_o z} - 1)}{q_o^2 (1+z)^2} \right) \quad (4)$$

$$g(z)^{-1} = \frac{H_o}{c} \left((1+z)^2 \sqrt{1 + 2q_o z} \right) \quad (5)$$

In this parameterization, two special cases are noteworthy. Clustering that remains constant in co-moving coordinates yields $\epsilon = \gamma - 3 \approx -1.2$. Clustering that remains fixed with respect to physical coordinates yields $\epsilon = 0$.

We use several different redshift distributions in our fitting procedure (all shown in Figure 6). The first is based on fits of the empirical function $dN(z)/dz \propto z^2 \exp(-(z/z_o)^2)$ to the CFRS data and its extrapolation to fainter magnitudes (Lilly *et al.* (1995); hereafter CFRS model). This parameterization provides a very good representation to the observed data (Brainerd & Smail (1997)) and allows one to use a smoothly varying function in the Limber equation, thus removing shot noise effects present in the actual data. The median redshifts for the CFRS-based $N(z)$ model are 0.095, 0.145, 0.260, 0.420, 0.540, 0.615, 0.690, 0.755, 0.810, and 0.865 for I_{median} mags of 16.5, 17.5, 18.5, 19.5, 20.5, 21.25, 21.75, 22.25, 22.75, and 23.25, respectively. The remaining $N(z)$ models are generated by integrating an evolving Schechter luminosity function in successive redshift shells (hereafter EvLF models) and within magnitude limits that correspond to our chosen subsamples. The evolution is assumed to be a pure luminosity evolution as represented by the Schechter LF parameters $\alpha = -1.1$, $M_I^*(z) = -20.9 + 5\log h - \beta z$, and $\beta = 1, 1.5, 2$. The β values were chosen to approximately bracket the CFRS model. All the models contain a significant fraction of high- z galaxies by $I = 23.5$: $\sim 30 - 65\%$ with $z > 1$ and $\sim 3 - 30\%$ with $z > 1.5$ for the EvLF models; 44% with $z > 1$ and 11% with $z > 1.5$ for the CFRS model.

For each $N(z)$ model, we find the best-fit to our $\omega(1')$ vs I magnitude data by identifying the combination of r_o and ϵ that minimize the χ^2 statistic. Table 4 and Figures 7 and 8 summarize the results of the fitting procedure. The best fit in the range $16 < I < 23$ using the CFRS $N(z)$ model gives $r_o = 5.6h^{-1}$ Mpc and $\epsilon = -0.20$. The best fits for the EvLF $N(z)$ models are $(r_o, \epsilon) = (3.8h^{-1} \text{ Mpc}, -0.80)$, $(3.8h^{-1} \text{ Mpc}, -1.40)$, and $(4.1h^{-1} \text{ Mpc}, -1.70)$ for $\beta = 1, 1.5$, and 2, respectively. If we fix the correlation length to be $5.5 \pm 1.5h^{-1}$ Mpc, a value that is typical of that found from local redshift surveys (*e.g.*, de Lapparent, Geller, & Huchra (1988), Jing, Mo, & Boerner (1998), Tucker *et al.* (1997)), the best fit ϵ values fall in the range $-0.4 \leq \epsilon \leq +1.3$. Restricting the fits to data with $I \leq 20$, in general, also yields more positive ϵ values and higher correlation lengths that are consistent with those from the above local redshift surveys (see columns 3 and 5 in Table 4). Fits to data in subsets between $I = 18$ and $I = 23$ are consistent with the results obtained using all data with $I \leq 23$. In other words, we see little change in the correlation length with magnitude for $18 \leq I \leq 23$ for a given redshift distribution. All fits were done assuming a slope of $\gamma = 1.8$ and $q_o = 0.1$ (for $q_o = 0.5$ the best fit r_o values are $\sim 7\%$ lower).

Figure 8 shows the reduced χ^2 contours for the four $N(z)$ models as functions of r_o and ϵ . Two things are clear from the χ^2 measurements. First, there is a significant covariance between r_o and ϵ – for a given redshift distribution, lower correlation lengths are coupled with lower ϵ values. Second, the best-fit is located within a fairly shallow minimum at least in the direction of the $r_o - \epsilon$ covariance. Thus, although the best fits prefer $\epsilon < 0$, positive values are included in the 1σ contours, albeit with correspondingly higher correlation lengths. We provide an approximate description of the covariance between r_o and ϵ by determining the best-fit line to the data within the 1σ contour. The fit is determined by computing the mean between the fits $r_o = f(\epsilon)$ and $\epsilon = f(r_o)$. The typical 1σ uncertainty in r_o at a given ϵ is $\pm 0.15h^{-1}$ Mpc and $\pm 0.23h^{-1}$ Mpc for the EvLF and CFRS models, respectively (for the full $I \leq 23$ dataset). The typical 1σ uncertainty in ϵ at a given r_o is ± 0.18 (for all models). These fit parameters are given in Table 4.

4.2. Dependence of ϵ on Angular Scale

Our large survey allows us to perform model fits at scales other than $1'$. We perform a similar analyses for $\theta = 0.5', 3', 10'$, and $30'$. The results are shown in Figure 9. Figure 10 shows the best fit ϵ value as a function of angular scale obtained when the CFRS redshift model is used. The results for the EvLF

redshift models are similar shape although there is a zeropoint shift in the ϵ values. For $I > 22$, there is a trend towards larger ϵ values as the angular scale decreases, perhaps suggesting that the clustering on the smallest scales evolves more rapidly. The uncertainties in ϵ on scales greater than 10 arcminutes are substantial, however, and the trend is not seen at $I \leq 21$. We show in the following section that there is a significant flattening of the slope of the correlation function when $I > 22$ as well. These two trends are not easily identified with any known observational or instrumental effects (see discussion below) but clearly a deeper, wide area survey is needed to confirm these results.

4.3. Dependence of the Slope on Magnitude

We find no significant dependence of the correlation function slope on magnitude for $I \leq 22$ as shown in Figure 11. Over this magnitude range and for $1' \leq \theta \leq 20'$ the best fit slope is $\delta = -0.80 \pm 0.02$. For our two faintest bins ($I > 22$), a flattening of the slope on angular scales $\theta \lesssim 5'$ is seen with $\delta = -0.48 \pm 0.04$ for $22 \leq I < 23$ (see Figure 3 and Table 3 as well). The trend is not explained by seeing or deblending effects as it is also seen in the subset of the data with the best resolution ($\text{FWHM} \leq 1.25''$). It could, in principle, be introduced by poorly calibrated frame to frame photometric zeropoint variations. However, our observing strategy enables us to measure and correct for these variations quite well (see §2) and any residual variations are not sufficient to introduce a flattening of this magnitude. Furthermore, the $22 \leq I < 22.5$ bin is still 1 magnitude brighter than the completeness limit. Experiments with simulated CCD data show that our object detection software is not dependent on the clustering properties of the objects. As an additional check, however, we compute $\omega(\theta)$ independently for the 4 quadrants of the survey, for the single run with the best atmospheric transparency, and for each individual CCD frame. We see the flattening in these subsamples as well. One would not expect an effect introduced by zeropoint miscalibration to survive all these experiments. This dependence has been seen in two other surveys at approximately the same magnitude and over the same angular scales as seen here. Neuschaffer & Windhorst (1995) report slopes of $\delta = -0.5$ by $g = 25$ based on two independent fields, each one covering 0.25 contiguous deg^2 . Campos *et al.* (1995) find best fit slopes of $\delta = -0.6$ and $\delta = -0.55$ for their $R \leq 22$ and $R \leq 23$ samples, respectively. There is a physical model that can be invoked to explain the flattening; we will summarize it in the next section. While it is intriguing that our results are roughly consistent with those seen in these two independent surveys done at different wavelengths, we remain cautious for now since the effect is only seen in our faintest bins. Other large, contiguous surveys now underway (Dey & Jannuzi 1997, Falco 1997) should provide an important check on this result. We note that the constraints on r_o and ϵ discussed above do not change if we exclude the two faintest points from the analysis.

5. Discussion

Our constraints on $\omega(\theta)$ reveal a dependence of its amplitude on median I magnitude that appears to fit the model of the redshift evolution of $\xi(r)$ parameterized as $\xi(r, z) = (\frac{r}{r_o})^{-\gamma}(1+z)^{-(3+\epsilon)}$. In fact, this model provides an acceptable representation of the data over the range $16 < I < 25$ if the results of Brainerd & Smail (1997) are also included in the fits. The decline in the amplitude of the correlation function (over a wide range of scales) with I magnitude is about 3 times steeper over the range $16 \lesssim I \lesssim 19$ than over the range $20 \lesssim I \lesssim 23$. The $N(z)$ distributions that yield good fits to magnitude- $\omega(\theta)$ relation typically have about 40% of the galaxies at $z > 1$ by $I = 23$, consistent with the conclusions of Brainerd & Smail (1997). A shallower decline in the amplitude of $\omega(\theta)$ with magnitude for $I \gtrsim 21$ can be induced

by the reduction of the proper volume element at higher z . Brainerd & Smail (1997) use this argument to support the assertion that a significant fraction of faint galaxies are at $z \gtrsim 1$. However, a high- z cutoff can also induce similar behavior since in this case the effective depth and redshift distribution are not changing dramatically as one goes to fainter limits. If such a cutoff were introduced, as noted by Lidman & Peterson (1996), by a selection bias *against* the detection of high- z galaxies a shallow decline in correlation length with magnitude would result. However, a strong redshift cutoff would also effect the number counts and the corresponding turnover in the counts is not seen (see also Woods & Fahlman (1997)). Given the excellent agreement we find with the HDF number counts, we conclude that a selection bias of this nature is not a significant problem for our sample.

Taken at face value, our best fits to the above model suggest the evolution of the spatial correlation function is relatively mild over the depth of the survey. When we allow r_o to be a free parameter in the fit, we obtain exponents in the range $-1.7 \lesssim \epsilon \lesssim -0.2$ with $3.8 \lesssim r_o \lesssim 5.6h^{-1}$ Mpc depending on the assumed redshift distribution. Growth in the clustering of galaxies (in proper coordinates) requires $\epsilon > 0$. The 95% confidence limits are substantial, nevertheless, given the strong covariance between r_o and ϵ . As Figure 8 demonstrates, our data are also consistent with $\epsilon > 0$ providing $4.5 \lesssim r_o \lesssim 7h^{-1}$ Mpc. If $\epsilon \gtrsim 1$ then values of $r_o \lesssim 4h^{-1}$ Mpc are strongly rejected. As already noted, redshift surveys of local galaxies find $r_o \sim 5.5 \pm 1.5h^{-1}$ Mpc.

The interpretation of the goodness of the fit to the above model, however, must take into account a number of additional selection effects that may mask more substantial evolution of the correlation function. It is known that low- z galaxy clustering depends on both the morphology and luminosity of the objects being studied (*e.g.*, Davis & Geller (1976), Moore *et al.* (1994), Loveday *et al.* (1995), Guzzo *et al.* (1997), Valotto & Lambas (1997)). The sense of these trends is that elliptical galaxies and more luminous galaxies tend to have larger correlation lengths than spiral galaxies and less luminous galaxies, respectively. We also know that the mean absolute luminosity of the objects in a flux-limited sample will increase with redshift. The relative insensitivity of our derived r_o values to I magnitude for galaxies with $I \geq 17$ could therefore be, in part, the result of two competing effects. As one goes fainter the mean redshift of the galaxies in the survey tends to increase. If galaxies at $0.5 \lesssim z \lesssim 1$ exhibit a similar luminosity dependent clustering as local galaxies and/or I -band selection enhances the elliptical galaxy fraction at these redshifts then it is possible that a decrease in the spatial correlation length with magnitude could be partially offset by the tendency for more luminous and/or early type galaxies to be more strongly clustered. This could also explain the observed preference for negative ϵ values (which suggests only modest clustering evolution). The precise evolution of ϵ and r_o with redshift is intimately connected to the density perturbation power spectrum and the galaxy merger rate (Moscardini *et al.* (1997)). The complexity of the dependence makes a unique theoretical interpretation the observational constraints problematic. None the less, the constraints are now solidly determined on degree-scales and less down to $I = 23$ from the present survey.

More stringent constraints on clustering evolution will require the addition of multiple passbands or redshift data. Efstathiou *et al.* (1991) report a marginal increase in the clustering amplitude as one selects redder passbands and posit that normal galaxies dominate the composition of fainter I -band selected galaxy samples as opposed to the weakly clustered faint galaxies, that appear to dominate U and B selected surveys. Lidman & Peterson (1996) also find a marginally significant color dependence, showing that red ($V - I > 1.5$) galaxies have a larger clustering amplitude than blue galaxies. Le Fevre *et al.* (1996) find no color dependence to the clustering properties of galaxies at $z > 0.5$ from an analysis of the CFRS data. They have also measured the spatial correlation function directly from their redshift data. They find a correlation length of $r_o = 1.57 \pm 0.09h^{-1}$ Mpc at $z \sim 0.5$ which, if they are sampling a mix

of galaxies similar to those in local redshift surveys, implies $0 < \epsilon < 2$. Our results are consistent with this ϵ range. From equation (2), we know $r_o(z) = r_o(0) (1+z)^{-(3+\epsilon)/\gamma}$. Using our best-fit results for the CFRS redshift distribution we, thus, find that $r(z = 0.5) \approx 3.0h^{-1}$ Mpc. Results for the EvLF redshift distribution models yield $r(z = 0.5) = 2.7 \pm 0.4h^{-1}$ Mpc. The CFRS galaxies were also I -band selected so any difference in results between the CFRS and our angular survey are due either to projection effects (which tend to wash out clustering) or the volume sampled as opposed to intrinsic differences between the galaxy population.

Connolly, Szalay, & Brunner (1998) determined the redshift dependence of the amplitude of $\omega(\theta)$ using photometric redshifts derived from the HDF survey. For $z > 0.4$, they find $r_o = 2.37h^{-1}$ Mpc and $\epsilon = -0.4^{+0.37}_{-0.65}$. However, in order to be consistent with low- z surveys, they would require $\epsilon \sim 2$. They suggest, therefore, that the expression for the evolution of the spatial correlation function, $\xi(r, z) = (\frac{r}{r_o})^{-\gamma}(1+z)^{-(3+\epsilon)}$, is not particularly good. Others have made similar claims based on poor fits to the $\omega(\theta)$ vs. magnitude relation. This is in contrast with the excellent fit we obtain extending over 7 magnitudes (Figure 7). We speculate that the discrepancy is caused by cosmic variance due to the small area used in previous measurements of the correlation function. Connolly, Szalay, & Brunner (1998) note that the HDF survey subtends only $800h^{-1}$ kpc at $z = 1$ ($q_o = 0.1$), a fraction of the galaxy correlation length. The CFRS is larger (five $10' \times 10'$ fields) but still covers a relatively small volume ($10'$ spans $3.1h^{-1}$ Mpc at $z = 1$). Hence, these surveys are also subject to the same sorts of problems associated with cosmic scatter and undersampling of LSS as small area angular surveys. Indeed, de Lapparent, Geller, & Huchra (1988) make a clear demonstration of this point at low- z : even in their redshift survey of ~ 1810 galaxies ($z \leq 0.05$) filling a volume of $5 \times 10^5 h^{-3}$ Mpc³, the density fluctuations caused by LSS prevent the determination of r_o by better than a factor of 2. Given that the deep, redshift probes sample roughly comparable volumes (but with the added complication that they stretch over a significant fraction of cosmic time), it seems optimistic to expect reliable constraints to be determined from the existing surveys. In fact, it is quite remarkable that the values obtained from them are in agreement with the local correlation length to within a factor of two. Not until much larger volumes are surveyed will the constraints on r_o at high redshift be robustly measured. If the results from direct measurements of the spatial correlation function at higher redshifts are ultimately accurate, however, and assuming their sample composition is not significantly different from the low redshift surveys, then the basic model may be in need of refinement.

One possible refinement, discussed in some detail already by Neuschaffer & Windhorst (1995), is to include a redshift-dependent spatial correlation function slope. This would be a natural consequence of models in which there is a scale dependence to the growth of structure. For example, if galactic scale structures grow significantly faster than structures on scales $\gtrsim 20h^{-1}$ Mpc the correlation function slope would steepen with time. This would also cause the slope of $\omega(\theta)$ to flatten at fainter magnitudes on small scales and, depending on the details of the density perturbation power spectrum and the merger rate, could also result in an increase in ϵ with redshift on small scales. Adopting the parameterization $\gamma(z) = 1.8(1+z_{med})^{-C}$ proposed by Neuschaffer & Windhorst (1995), implies $C = 0.35 \pm 0.10$ which is consistent with their limit. As Neuschaffer & Windhorst (1995) demonstrate, values in the range $C \lesssim 0.4$, are consistent with structure formation models which have significant power on co-moving scales of $\lesssim 10h^{-1}$ Mpc but disfavor models with little small scale power such as HDM. However, since the flattening is only seen at $I \gtrsim 22$, the above parameterization of the slope redshift dependence is not particularly good – there appears to be no real redshift dependence to the slope until $z_{med} \gtrsim 0.6$.

6. Summary

We have produced an I -band selected catalog of $\sim 710,000$ galaxies for studying the evolution of structure out to $z \sim 1$. Our survey puts new and stringent limits on the magnitude dependence of the two-point angular correlation function. The survey is the first of a new generation of deep, wide-area imaging surveys made feasible by large-format CCDs and mosaic cameras. The key results presented in this paper are

1. Galaxy number counts are consistent with modest evolution in luminosity ($0.5 - 1$ mag, depending on Ω_o) and/or density (factor of $1.5 - 2$). The counts are consistent with the F814W HDF counts in the range $21 < I \leq 24$ suggesting that the HST-based catalog does not contain a substantial number of sub-galactic components in this flux range.
2. The two-point correlation function agrees remarkably well with that of the APM in the magnitude range common to both surveys. At the faint end, our measurements of $\omega(\theta)$ are consistent with those of Brainerd & Smail (1997), who have measured $\omega(\theta)$ down to $I = 25$. The large contiguous size of our survey minimizes the effects of cosmic scatter and provides a firm determination of $\omega(\theta)$ over 7 magnitudes.
3. The amplitude of the two-point angular correlation function decreases monotonically with increasing magnitude over the range $16 \leq I \leq 23$. The decline is well fit by a redshift dependence of the spatial correlation function parameterized as $(1+z)^{-(3+\epsilon)}$. Our best fit correlation lengths for galaxies with $I \leq 20$ are consistent with those from low- z redshift surveys. At fainter magnitudes we find correlation lengths in the range $3.8 \leq r_o \leq 5.5h^{-1}$ Mpc depending on the assumed redshift distribution. If $\epsilon \gtrsim 1$ then we strongly reject $r_o \lesssim 4h^{-1}$ Mpc for our $I > 20$ sample. However, more negative ϵ values are preferred at $I > 20$, suggesting the effective clustering is not evolving as rapidly as linear perturbation theory predicts. The possible preference for inclusion of more luminous and/or early type galaxies at fainter magnitudes in the survey could explain this trend.
4. Our derived correlation length at $z \approx 0.5$ is about a factor of 2 larger than that derived from the CFRS. While a complete physical interpretation of our results requires additional color and redshift data, it is also clear that the volumes sampled by existing deep, redshift probes are inadequate to properly constrain the two-point spatial correlation function to better than the above difference. If the galaxy population sampled at $I \gtrsim 20$ is similar to that in the CFRS, then our deprojection of $\xi(r)$ may indeed be more accurate by virtue our reduced sensitivity to cosmic scatter.
5. For $I \leq 22$, the mean value of power-law slope of $\omega(\theta)$ is -0.80 ± 0.02 and is independent of magnitude. We find a slope of $\delta \approx -0.5$ is a better fit to the $I > 22$ data, however. This flatter slope is consistent with the results of Campos *et al.* (1995) and Neuschaffer & Windhorst (1995). We also detect an increase in ϵ on scales less than 1 arcminute for $I > 22$. We can identify no instrumental or software-related cause for these effects but remain cautious in interpreting the full signals as real phenomena. Such trends are, however, consistent with structure formation models in which small scale power increases more rapidly than power on scales larger than $\sim 10h^{-1}$ Mpc.

Special thanks go to the KPNO TAC for their generous support of this research. We thank John Hoessel for help with the initial project proposal and Ralph Shuping for providing essential photometric calibration data. We thank the referee for helpful comments which improved the clarity of this paper. M.P. acknowledges support from the STScI's Director's Discretionary Research Fund. I.S. was supported by

DOE and NASA through grant NAG-5-2788 at Fermilab and by the PPARC rolling grant for Extragalactic Astronomy and Cosmology at Durham.

REFERENCES

- Babul, A., & Ferguson, H. 1996, *ApJ*, 458, 100
- Brainerd, T., & Smail, I. 1997, *ApJ Letters*, in press (see also astro-ph/9712276)
- Campos, A., Yepes, G., Carlson, M., Klypin, A. A., Moles, M., & Joergensen, H. 1995, Clustering in the Universe, S. Maurogordato, C. Balowski, C. Tao, & J. Trán Thanh Ván (eds.), pp. 403-406
- Cohen, J. G., Cowie, L. L., Hogg, D. W., Songaila, A., Blanford, R., Hu, E. M., & Shobbell, P. 1996, *ApJ*, 471, L5
- Colley, W. N., Rhoads, J. E., Ostriker, J. P., & Spergel, D. N. 1996, *ApJ*, 473, L63
- Connolly, A. J., Szalay, A. S., Koo, D., Romer, K. A., Holden, B., Nichol, R. C., Miyaji, T. 1996, *ApJ*, 473, L67
- Connolly, A. J., Szalay, A. S., & Brunner, R. J. 1998, *ApJ*, submitted.
- Croft, R. A. C.; Dalton, G. B.; Efstathiou, G.; Sutherland, W. J.; Maddox, S. J 1997, *MNRAS*, 291, 305
- Dalton, G. B.; Croft, R. A. C.; Efstathiou, G.; Sutherland, W. J.; Maddox, S. J.; Davis, M. 1994, *MNRAS*, 271, 47
- de Lapparent, V. L., Geller, M. J., & Huchra, J. P. 1988, *ApJ*, 332, 44
- Dey, A., & Jannuzi, B. 1997, private comm.
- Davis, M., & Geller, M. J. 1976, *ApJ*, 208, 13
- Efstathiou G., Bernstein, G., Tyson, J.A., Katz, N., & Guhathakurta, P. 1991, *ApJ*, 380, L47
- Falco, E. 1997, private comm.
- Ferguson, H., & Babul, A. 1998, astro-ph/9801057.
- Gardner, J. P., Sharples, M. R., Carrasco, B. E., & Frenk, C. S. 1996, *MNRAS*, 282, L1
- Giavalisco, M., Steidel, C. C., Adelberger, K. L., Dickinson, M. E., Pettini, M., & Kellogg, M. 1997, *ApJ*, submitted
- Groth, E. J. & Peebles, P.J.E. 1977, *ApJ*, 217, 385
- Gunn, J., Hoessel, J., Oke, J. B. 1986, *ApJ*, 306, 30
- Guzzo, L.; Strauss, M. A.; Fisher, K. B.; Giovanelli, R.; & Haynes, M. P. 1997, *ApJ*, 489, 37
- Jing, Y. P., Mo, H. J., Boerner, G. 1998, *ApJ*, 494, 1
- Landy, S.D., & Szalay, A. 1993, *ApJ*, 412, 64
- Le Fevre, O., Crampton, D., Lilly, S., Hammer, F., & Tresse, L. 1995, *ApJ*, 455, 60
- Le Fevre, O., Hudon, D., Lilly, S., Crampton, D., Hammer, F., & Tresse, L. 1996, *ApJ*, 461, 534
- Lidman, C., & Peterson, B. 1996, *MNRAS*, 279, 1357

Lilly, S., Cowie, L. L., & Gardner, J. P., 1991, ApJ, 369, 79

Lilly, S., Tresse, L., Hammer, F., Crampton, D., & Le Fevre, O. 1995, ApJ, 455, 108

Limber, D. N. 1953, ApJ, 117, 134

Loveday, J., Maddox, S. J., Efstathiou, G., & Peterson, B. A. 1995, ApJ, 442, 457

Maddox, S. J., Efstathiou, G., & Sutherland, W. J. 1996, MNRAS, 283, 1227

Moore, B., Frenk, C. S., Efstathiou, G., Saunders, W. 1994, MNRAS, 269, 742

Moscardini, L., Coles, P., Lucchin, F., & Sabino, M. 1997, astro-ph 9712184 (v3).

Neuschaffer, L. W., & Windhorst, R. A. 1995, ApJ, 439, 14.

Peebles, P.J.E. 1980, The Large Scale Structure of the Universe (Princeton: Princeton University Press)

Postman, M., Huchra, J. P., & Geller, M. J. 1992, ApJ, 384, 404

Postman, M., Lubin, L., Gunn, J., Oke, J. B., Hoessel, J., Schneider, D., & Christensen, J. 1996 AJ, 111, 615.

Postman, M., Lauer, T. R., & Oegerle, W. 1998, in preparation

Smail, I., Hogg, D. W., Yan, L., Cohen, J., 1995, ApJ, 449, 105

Steidel, C. C., Adelberger, K. L., Dickinson, M. E., Giavalisco, M., Pettini, M., & Kellogg, M. 1998, ApJ, 492, 428

Szapudi, I., Postman, M., Lauer, T. R., & Oegerle, W. 1998, in preparation

Szapudi, I., & Columbi, S. 1996, ApJ, 470, 131

Tucker, D. L., Oemler, A., Kirshner, R. P., Lin, H., Shectman, S. A., Landy, S. D., Schechter, P. L., Muller, V., Gottlober, S., Einasto, J. 1997, MNRAS, 285, 5

Valdes, F. 1982, Proc. SPIE, 331, 465

Valotto, C. A., & Lambas, D. G., 1997, ApJ, 481, 594

Williams *et al.* 1996, AJ, 112, 1335

Woods, D., & Fahlman, G. 1997, ApJ, 490, 11

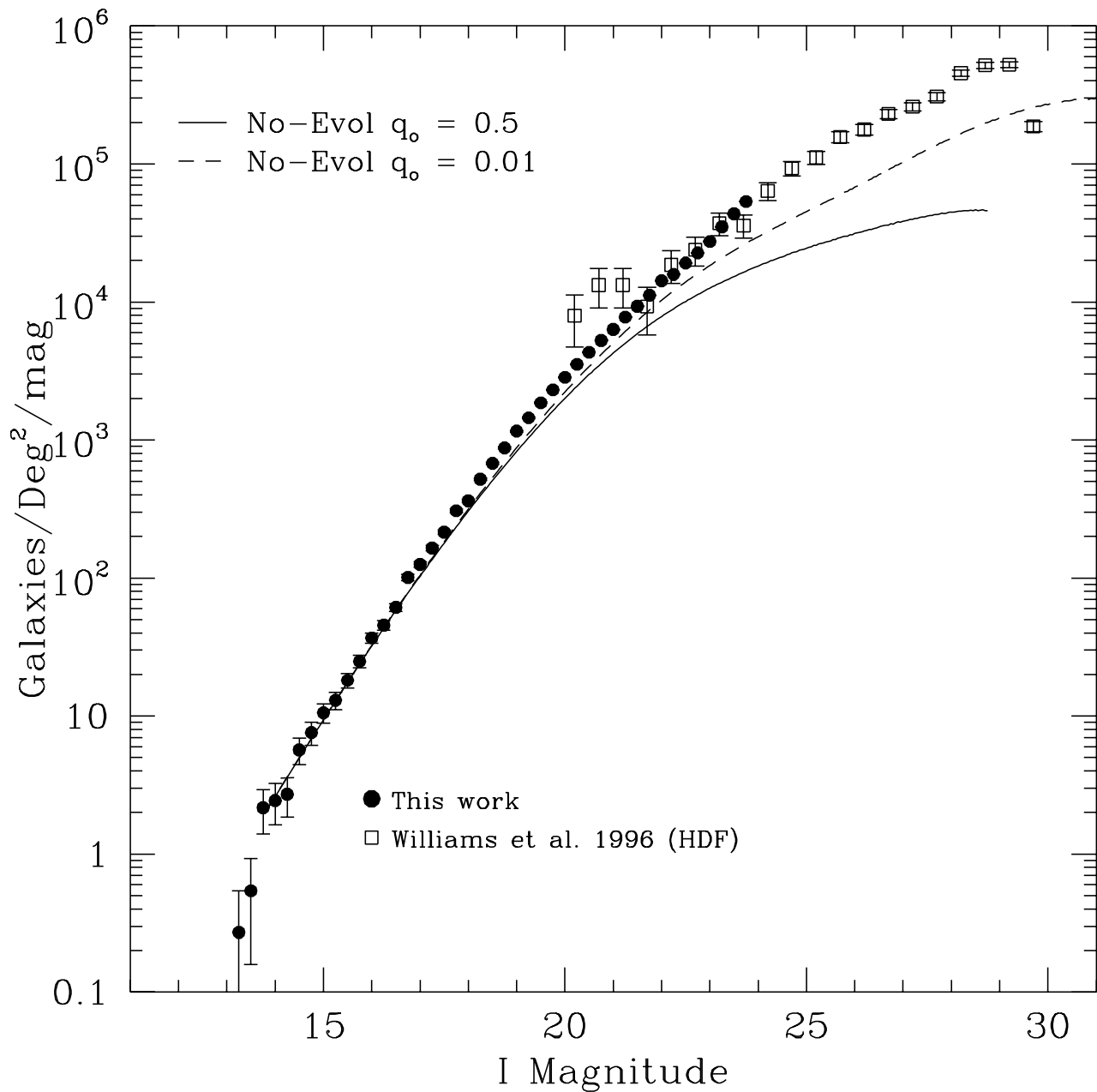


Fig. 1.— The differential galaxy surface density as a function of isophotal I magnitude. The I -band counts from the Hubble Deep Field (open circles; Williams *et al.* (1996)) are shown as well. The models (dashed and solid lines) are from Ferguson & Babul (1998).

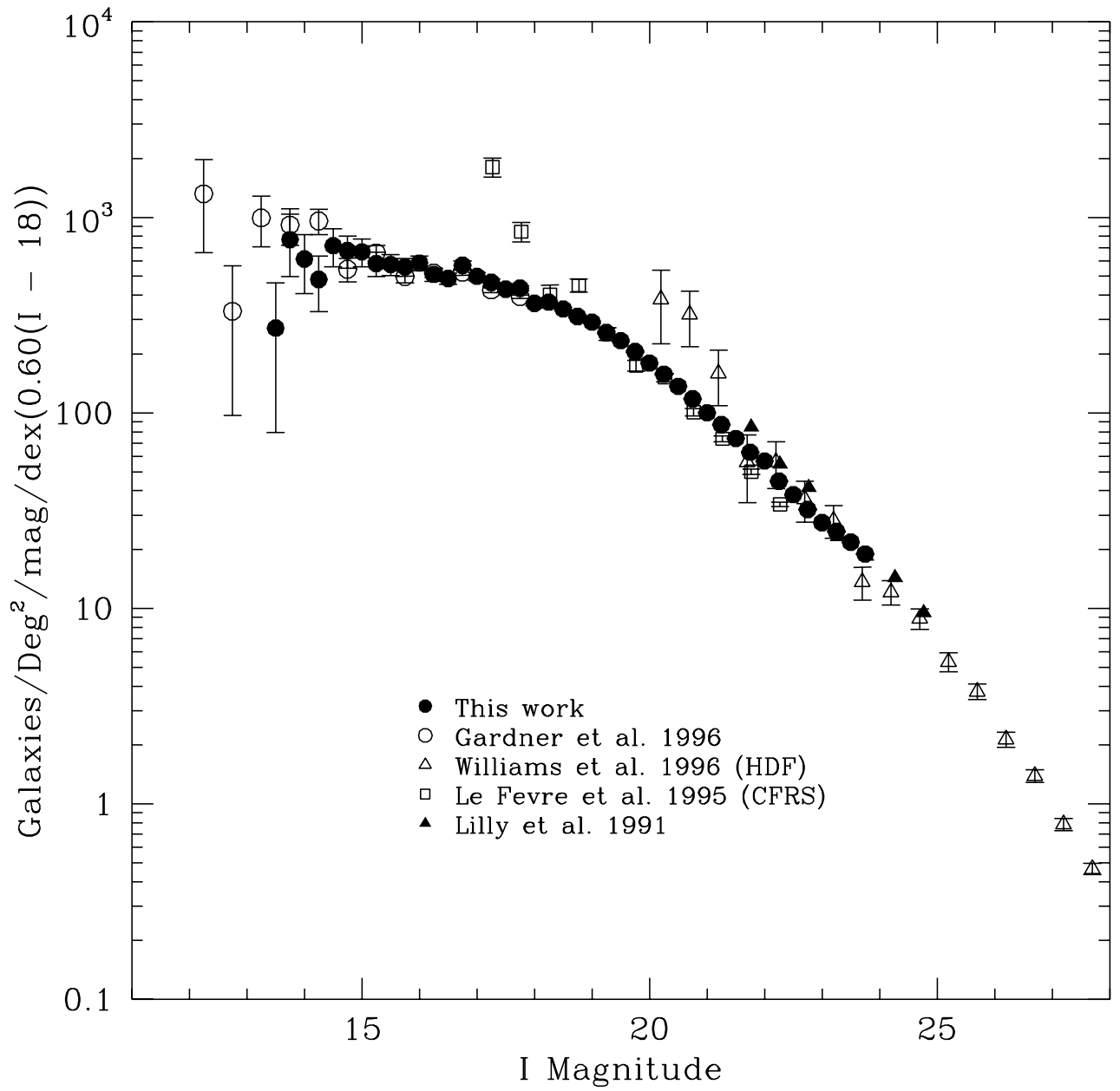


Fig. 2.— The differential galaxy surface density as a function of isophotal I magnitude for various surveys. Counts have been normalized by $\text{dex}(0.6(I - 18))$ to enhance small variations and departures from the expectations of Euclidean space.

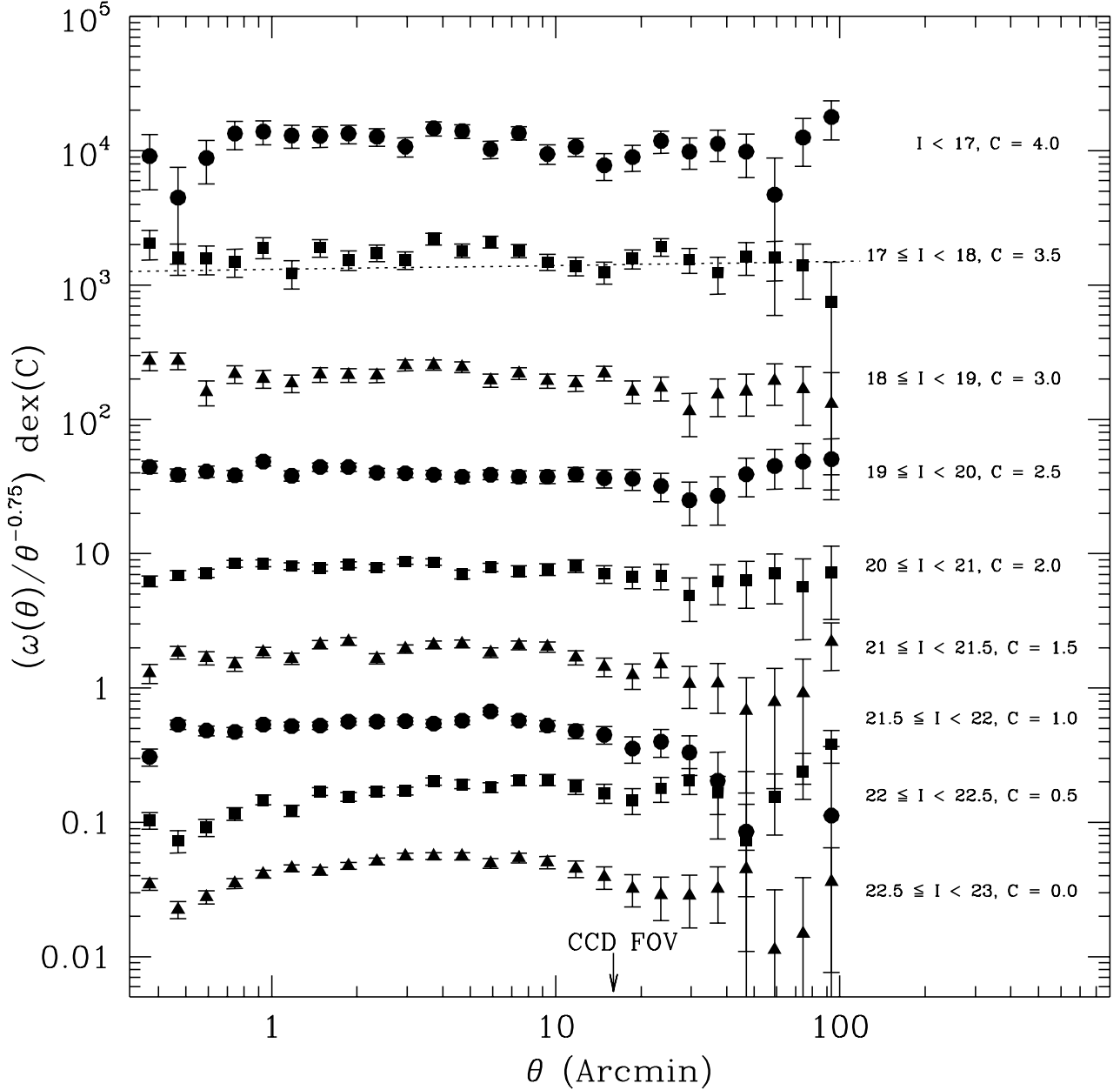


Fig. 3.— The two-point angular correlation functions, normalized by $\theta^{-0.75}$, for $17 \leq I \leq 23$. Results for each magnitude range are vertically offset by 0.5 dex, as well, for clarity (the value of each offset is shown explicitly on plot). The best-fit power law for the APM $17 < b_J < 20$ galaxy sample is shown as a dashed line (its vertical offset is the same as that for the $17 \leq I < 18$ sample). An arrow denotes the CCD field of view.

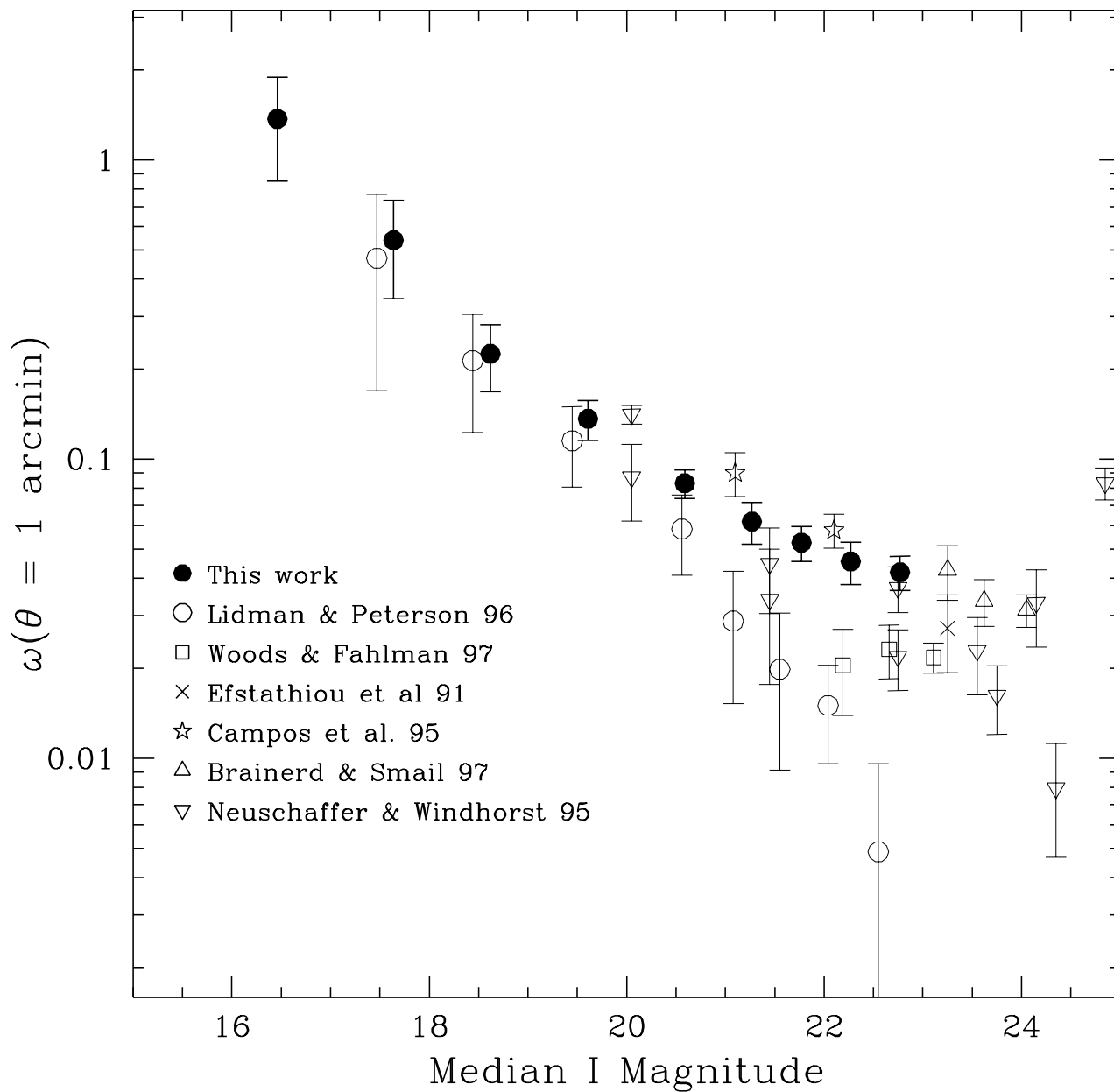


Fig. 4.— Amplitude of $\omega(\theta)$ at $1'$ vs. median I magnitude. Our results are the filled circles. Other recent measurements are also shown.

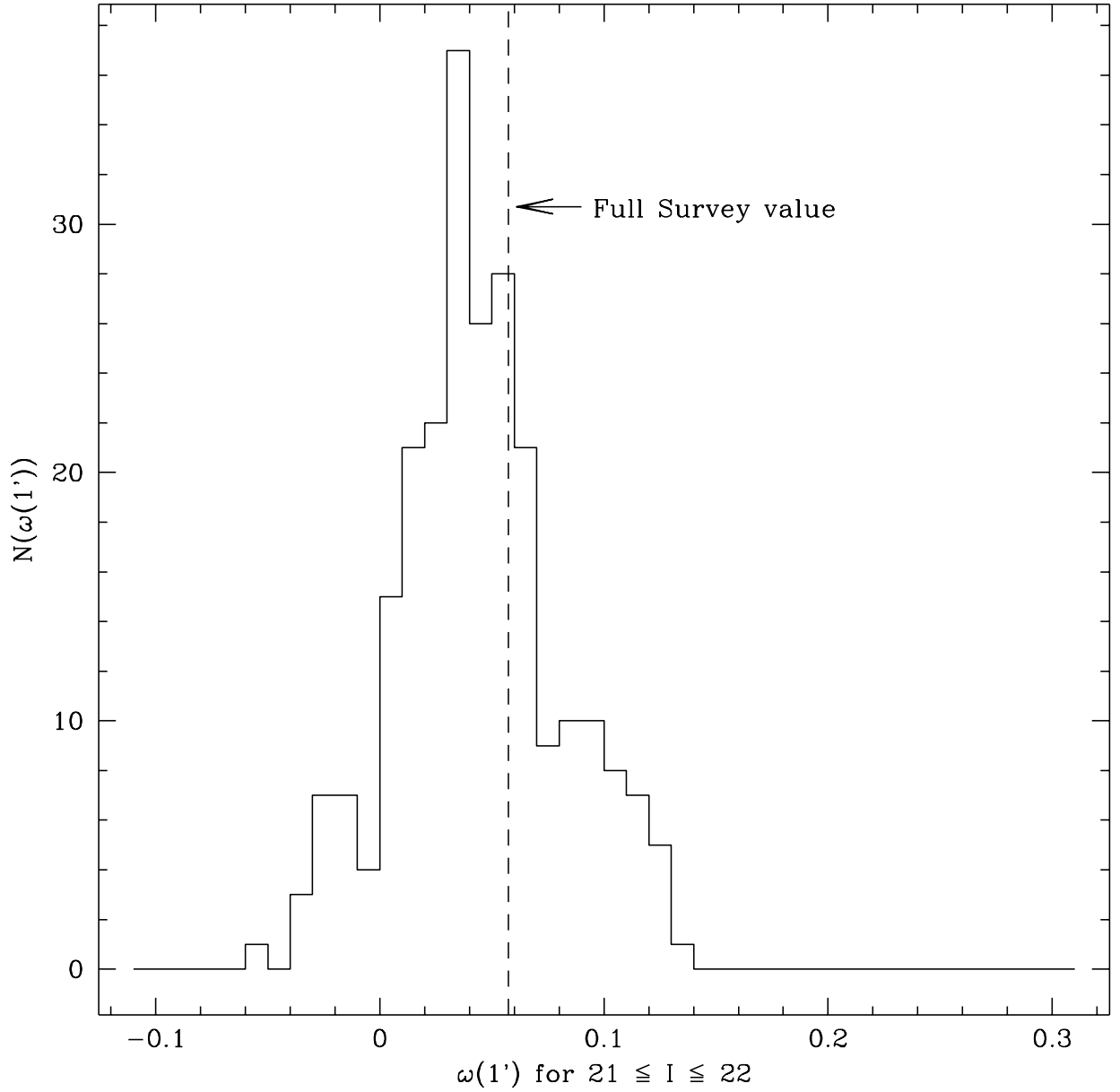


Fig. 5.— The histogram of $\omega(1')$ in the range $21 \leq I \leq 22$ for 250 independent $16' \times 16'$ CCD fields. The mean value is 0.045 but the variance is substantial owing to significant cosmic scatter on this scale at these magnitudes. The $\sim 20\%$ offset between the mean $\omega(1')$ for the independent CCD fields and that for full survey is entirely consistent with the uncertainties in the small field IC correction.

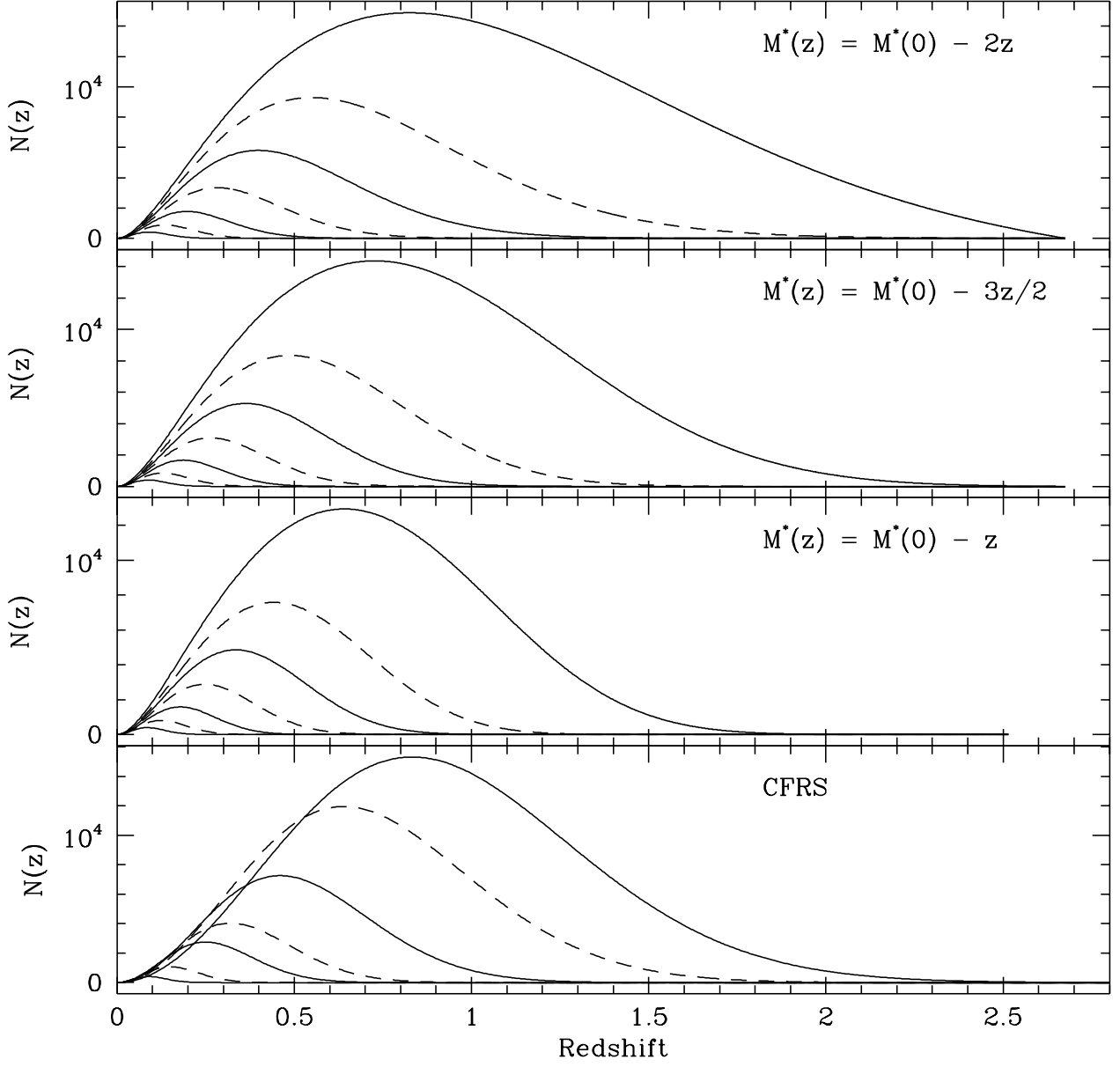


Fig. 6.— The differential redshift distributions for the CFRS model and the evolving luminosity function (EvLF) models for the magnitude intervals $16 \leq I < 17$, $17 \leq I < 18$, $18 \leq I < 19$, $19 \leq I < 20$, $20 \leq I < 21$, $21 \leq I < 22$, and $22.5 \leq I < 23.5$. The EvLF models assume a Schechter luminosity function with $\alpha = -1.1$, $M_I^*(z) = -20.9 + 5 \log h - \beta z$, and $\beta = 1, 1.5, 2$.

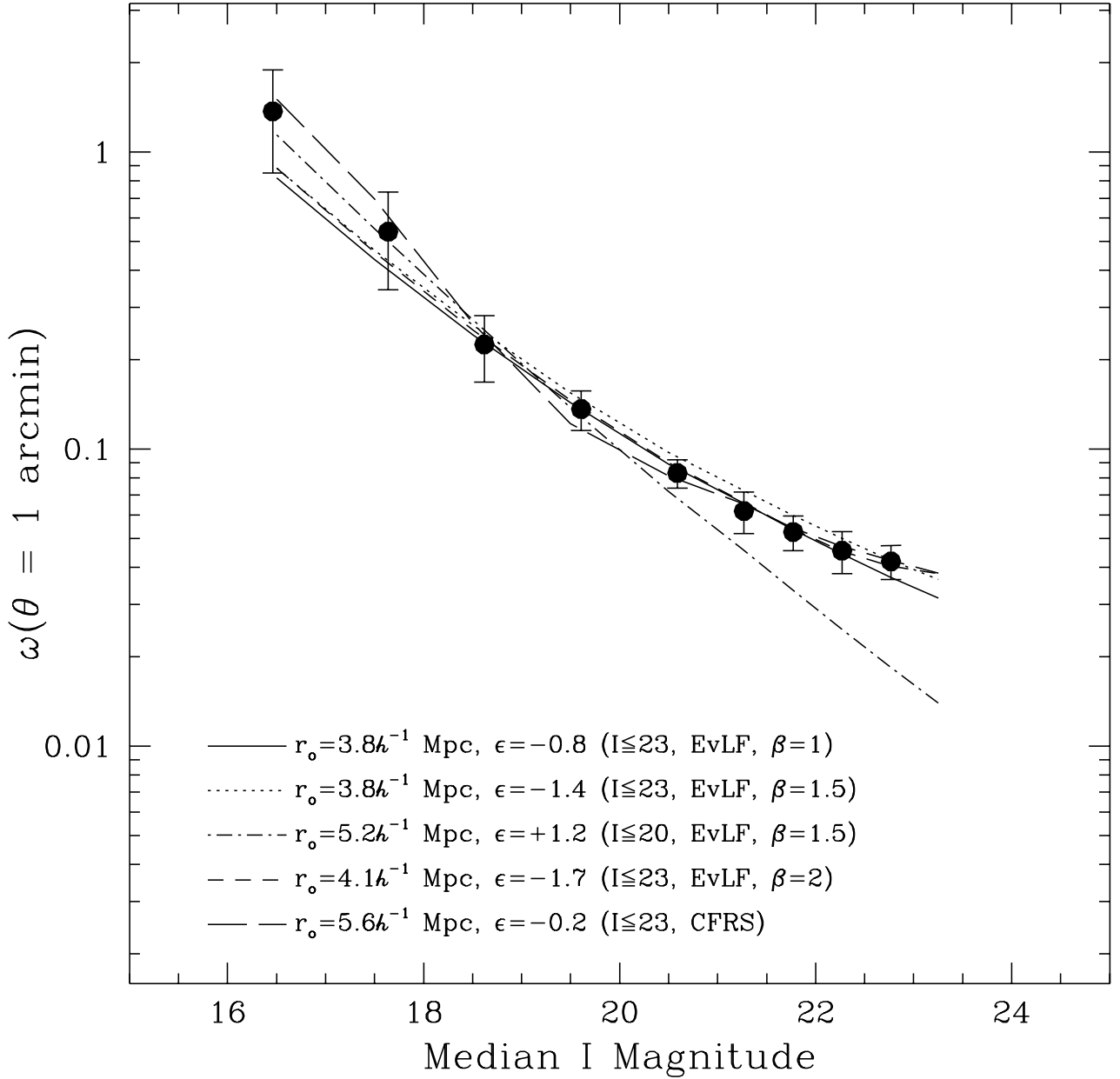


Fig. 7.— Best fits to our $\omega(1')$ vs I mag data using a Limber deprojection and various plausible redshift distributions. In the case of the EvLF $\beta = 1.5$ $N(z)$ model, we show fits to all the data and to just data with $I \leq 20$. Fits to data with $I \geq 20$ give similar results as those done using all data.

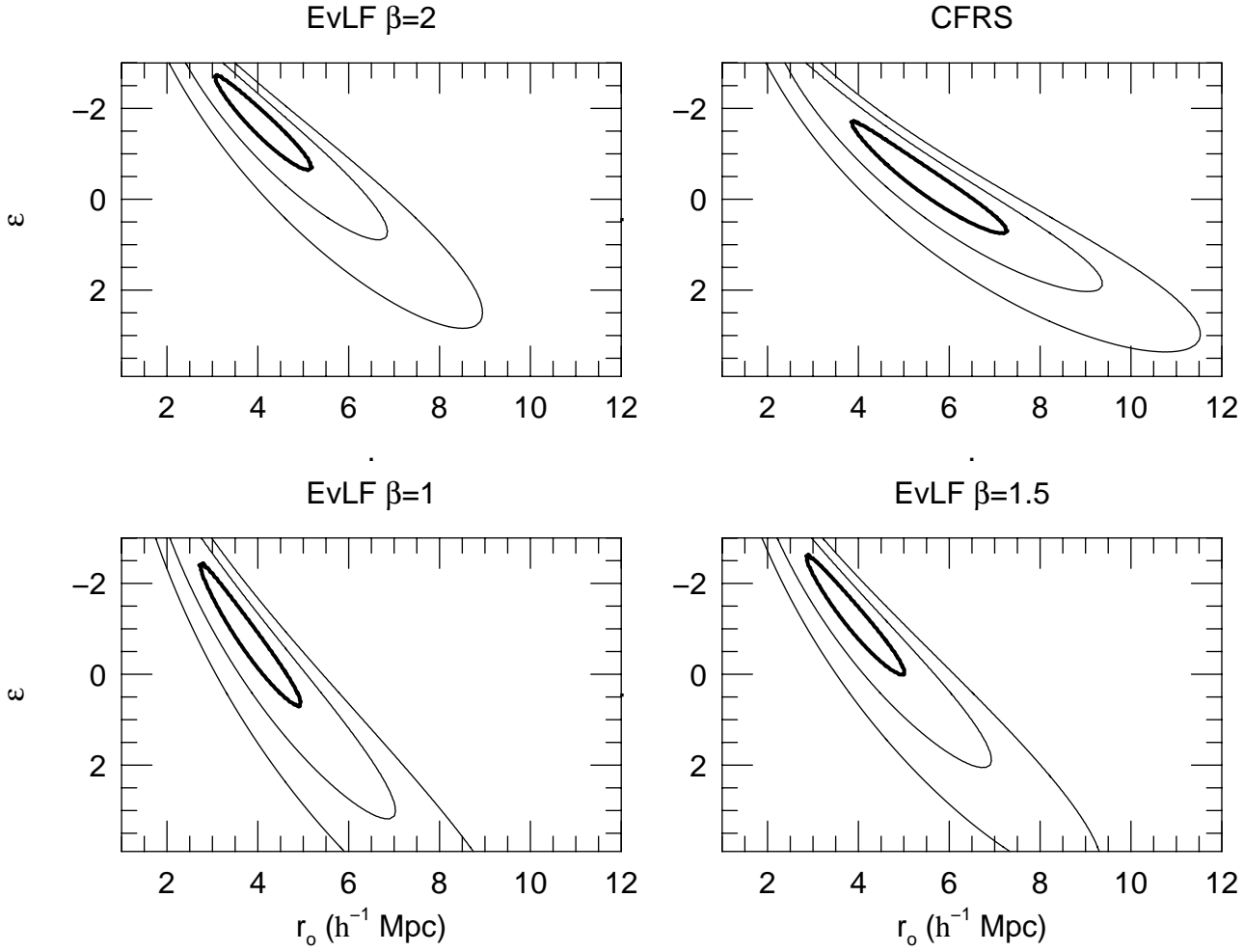


Fig. 8.— The reduced χ^2 contours for the fits to equation 1 using the EvLF ($\beta = 1, 1.5, 2$) and CFRS redshift distributions. Results shown here are for correlation amplitudes at 1 arcminute and $I_{\text{median}} \leq 23$. The 1σ (heavy line), 2σ , and 3σ contours are shown.

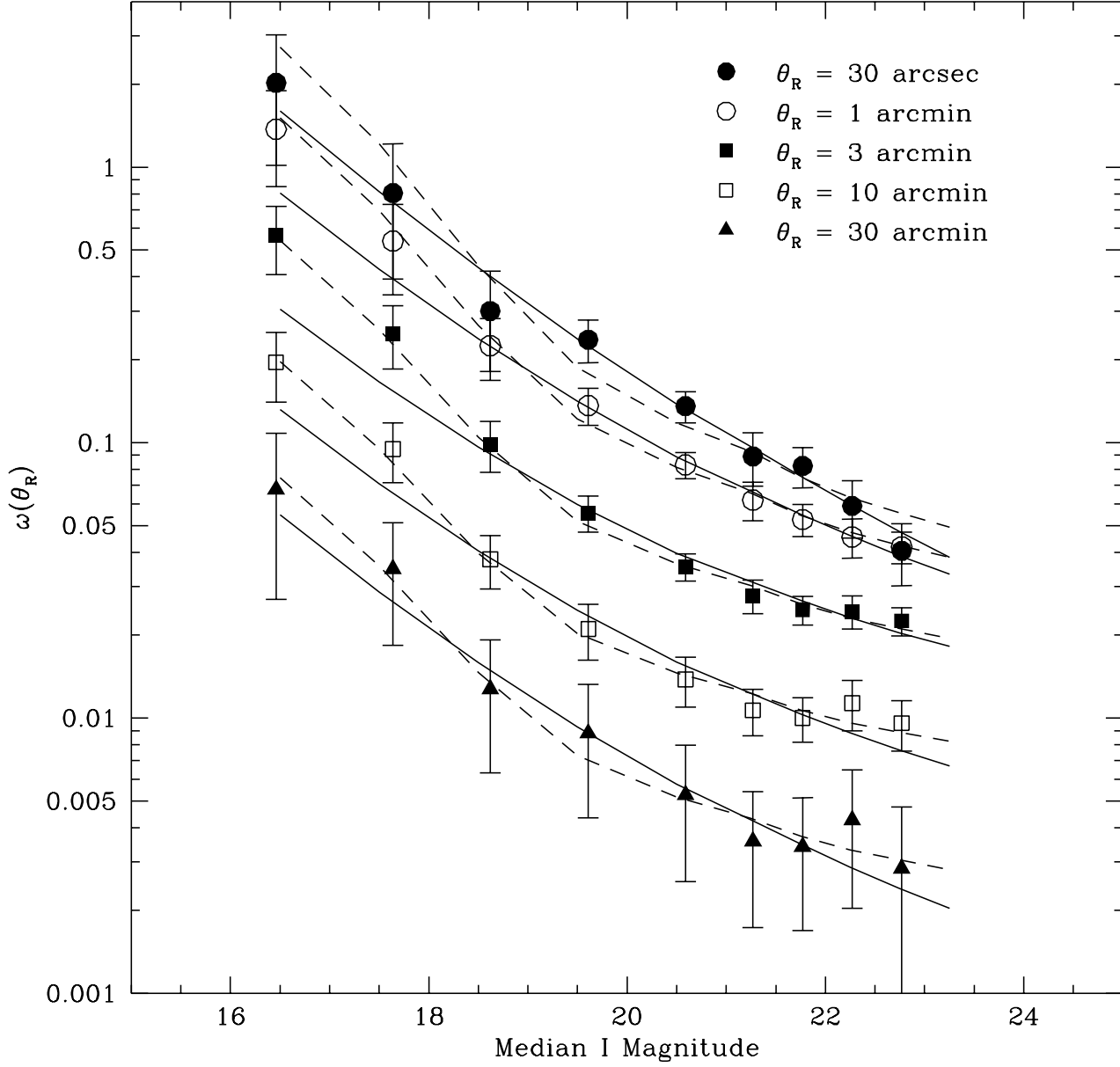


Fig. 9.— The amplitude of $\omega(\theta_R)$ as a function of median I magnitude for $\theta_R = 0.5', 1', 3', 10',$ and $30'$. Data have been corrected for integral constraint and stellar contamination. Best-fit models using the EvLF $\beta = 1.5$ and CFRS redshift distributions are shown as solid and dashed lines, respectively.

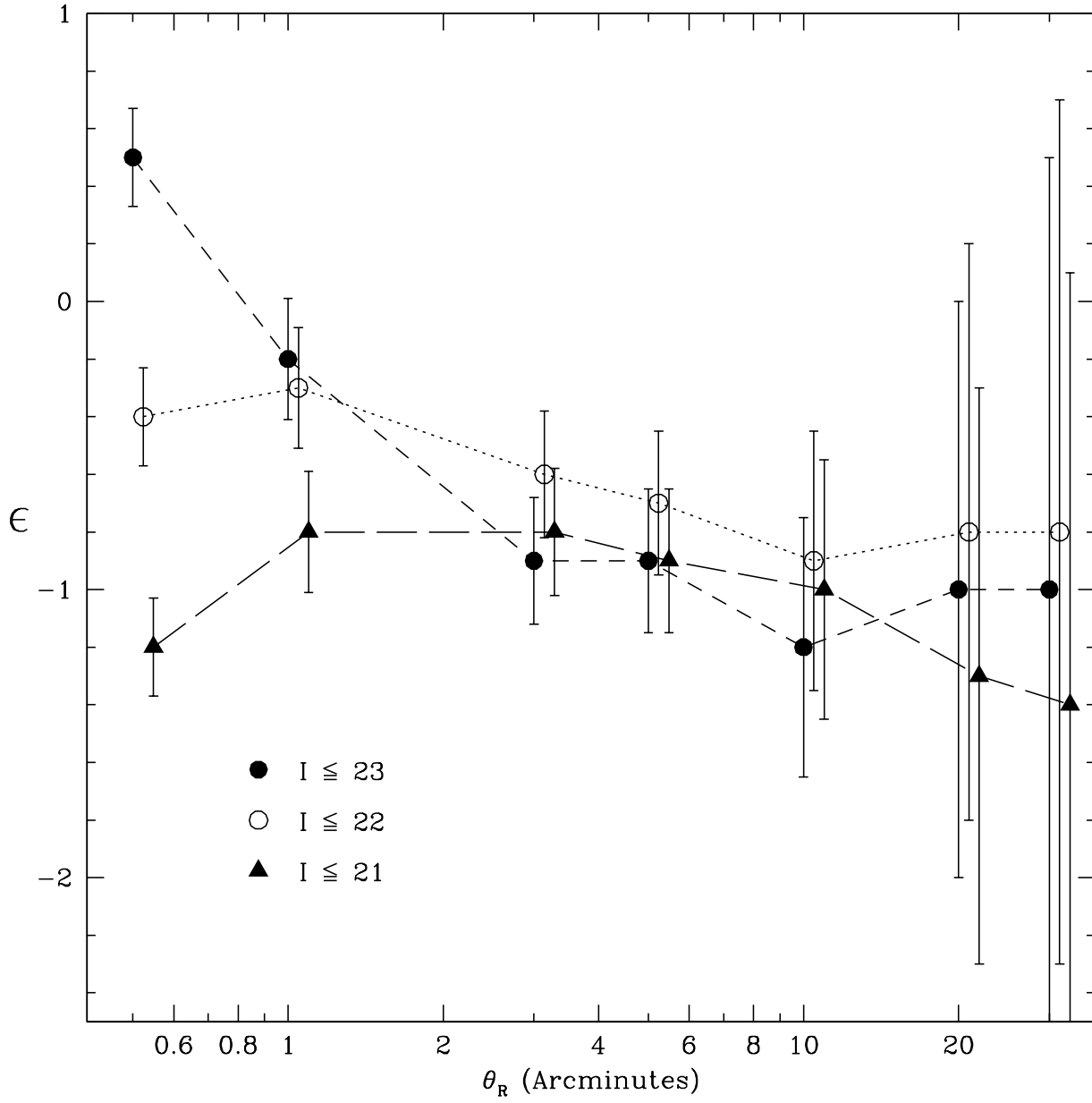


Fig. 10.— The best-fit ϵ value as a function of angular scale for data with $I \leq 21$, $I \leq 22$, and $I \leq 23$. The results shown are for the CFRS redshift distribution model. Results for the EvLF models are similar in shape but are offset vertically relative to the CFRS fits.

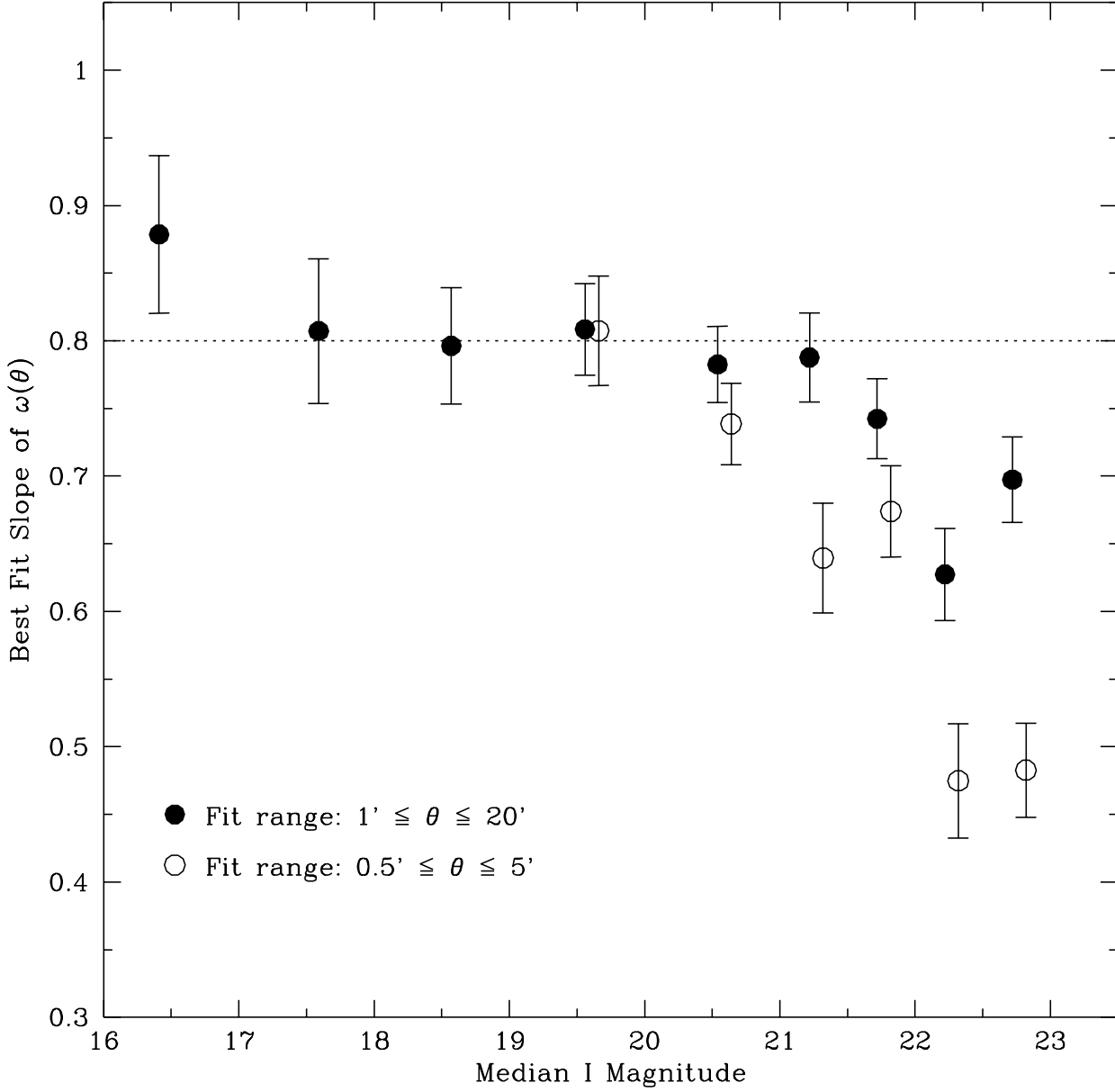


Fig. 11.— The best fit power law slope of the two-point correlation function as a function of I magnitude. The results for two different angular fitting limits are shown. The dashed line shows the mean slope derived for $I \leq 22$.

Table 1. Differential I -band Galaxy Counts

I mag	$\log(N)^a$	$\log(N_{\text{Cor}})^a$	σ_{high}^b	σ_{low}^b	I mag	$\log(N)^a$	$\log(N_{\text{Cor}})^a$	σ_{high}^b	σ_{low}^b
13.25	-0.5671	-0.5671	0.3010	0.5671	18.75	2.9433	2.9433	0.0076	0.0077
13.50	-0.2661	-0.2661	0.2323	0.5333	19.00	3.0641	3.0641	0.0066	0.0067
13.75	0.3360	0.3360	0.1315	0.1895	19.25	3.1613	3.1613	0.0059	0.0060
14.00	0.3872	0.3872	0.1249	0.1761	19.50	3.2696	3.2696	0.0052	0.0053
14.25	0.4329	0.4329	0.1193	0.1651	19.75	3.3633	3.3633	0.0047	0.0047
14.50	0.7551	0.7551	0.0857	0.1069	20.00	3.4547	3.4547	0.0042	0.0043
14.75	0.8801	0.8801	0.0752	0.0910	20.25	3.5482	3.5482	0.0038	0.0038
15.00	1.0240	1.0240	0.0645	0.0758	20.50	3.6360	3.6360	0.0034	0.0035
15.25	1.1142	1.1142	0.0586	0.0677	20.75	3.7218	3.7218	0.0031	0.0031
15.50	1.2590	1.2590	0.0501	0.0566	21.00	3.8007	3.8007	0.0028	0.0029
15.75	1.3967	1.3967	0.0431	0.0478	21.25	3.8904	3.8904	0.0026	0.0026
16.00	1.5665	1.5665	0.0357	0.0389	21.50	3.9690	3.9690	0.0023	0.0023
16.25	1.6582	1.6582	0.0323	0.0349	21.75	4.0486	4.0486	0.0021	0.0021
16.50	1.7870	1.7870	0.0280	0.0299	22.00	4.1196	4.1437	0.0019	0.0019
16.75	2.0046	2.0046	0.0219	0.0231	22.25	4.1825	4.2000	0.0027	0.0027
17.00	2.0985	2.0985	0.0197	0.0207	22.50	4.2579	4.2820	0.0024	0.0024
17.25	2.2175	2.2175	0.0173	0.0180	22.75	4.3222	4.3554	0.0022	0.0022
17.50	2.3327	2.3327	0.0151	0.0157	23.00	4.3873	4.4385	0.0020	0.0020
17.75	2.4875	2.4875	0.0127	0.0131	23.25	4.4549	4.5438	0.0018	0.0018
18.00	2.5600	2.5600	0.0117	0.0120	23.50	4.5166	4.6383	0.0016	0.0016
18.25	2.7164	2.7164	0.0098	0.0100	23.75	4.5768	4.7282	0.0015	0.0015
18.50	2.8314	2.8314	0.0086	0.0088					

^a N and N_{Cor} are the differential galaxy counts before and after correction for survey incompleteness, respectively. The units are galaxies $\text{deg}^{-2} \text{mag}^{-1}$.

^bThe 1-sigma Poisson errors in $\log(N_{\text{Cor}})$.

Table 2. Angular Two-Point Correlation Function ^a

θ	$I < 17$	$17 \leq I < 18$	$18 \leq I < 19$	$19 \leq I < 20$	$20 \leq I < 21$	$21 \leq I < 21.5$	$21.5 \leq I < 22$	$22 \leq I < 22.5$	$22.5 \leq I < 23$
0.37'	192 ± 84.5	136 ± 33.8	57.4 ± 8.96	29.4 ± 3.02	13.1 ± 1.23	8.56 ± 1.36	6.46 ± 0.94	6.87 ± 0.98	7.28 ± 0.72
0.47	79.2 ± 53.9	89.2 ± 23.4	48.3 ± 6.94	21.7 ± 2.32	12.2 ± 0.98	10.3 ± 1.10	9.44 ± 0.77	4.08 ± 0.77	3.96 ± 0.57
0.59	131 ± 46.8	74.0 ± 17.8	23.7 ± 5.00	19.2 ± 1.85	10.7 ± 0.78	7.86 ± 0.86	7.16 ± 0.61	4.31 ± 0.62	4.14 ± 0.46
0.74	167 ± 40.2	59.2 ± 14.1	27.2 ± 4.08	15.1 ± 1.44	10.6 ± 0.62	5.96 ± 0.68	5.90 ± 0.48	4.60 ± 0.50	4.39 ± 0.37
0.94	146 ± 29.7	63.5 ± 11.3	21.2 ± 3.19	16.2 ± 1.17	8.96 ± 0.50	6.16 ± 0.55	5.64 ± 0.39	4.90 ± 0.41	4.34 ± 0.30
1.18	115 ± 22.4	34.3 ± 8.20	16.5 ± 2.51	10.7 ± 0.92	7.18 ± 0.40	4.63 ± 0.44	4.61 ± 0.31	3.43 ± 0.33	4.04 ± 0.25
1.48	95.7 ± 16.9	44.7 ± 6.76	16.1 ± 2.00	10.4 ± 0.74	5.85 ± 0.33	4.97 ± 0.35	3.92 ± 0.25	3.99 ± 0.27	3.23 ± 0.21
1.87	84.1 ± 13.3	30.6 ± 5.16	13.4 ± 1.59	8.74 ± 0.60	5.19 ± 0.28	4.42 ± 0.29	3.52 ± 0.21	3.07 ± 0.23	2.99 ± 0.17
2.35	67.1 ± 10.2	29.0 ± 4.12	11.2 ± 1.27	6.70 ± 0.50	4.17 ± 0.23	2.76 ± 0.23	2.96 ± 0.17	2.83 ± 0.19	2.70 ± 0.15
2.96	47.7 ± 7.82	21.6 ± 3.23	11.2 ± 1.03	5.59 ± 0.42	3.91 ± 0.20	2.75 ± 0.19	2.51 ± 0.15	2.41 ± 0.17	2.48 ± 0.13
3.72	54.8 ± 6.50	26.1 ± 2.66	9.51 ± 0.84	4.59 ± 0.36	3.24 ± 0.18	2.47 ± 0.16	2.03 ± 0.13	2.39 ± 0.15	2.09 ± 0.12
4.69	44.1 ± 5.17	17.9 ± 2.11	7.72 ± 0.69	3.71 ± 0.31	2.20 ± 0.17	2.12 ± 0.14	1.80 ± 0.11	1.92 ± 0.14	1.76 ± 0.11
5.90	27.1 ± 4.06	17.6 ± 1.75	5.17 ± 0.58	3.25 ± 0.28	2.09 ± 0.16	1.53 ± 0.13	1.77 ± 0.10	1.53 ± 0.13	1.31 ± 0.11
7.43	30.2 ± 3.49	12.7 ± 1.45	4.89 ± 0.50	2.64 ± 0.26	1.66 ± 0.15	1.47 ± 0.11	1.28 ± 0.10	1.44 ± 0.12	1.21 ± 0.10
9.35	17.7 ± 2.93	8.81 ± 1.23	3.64 ± 0.43	2.22 ± 0.25	1.43 ± 0.14	1.20 ± 0.11	0.98 ± 0.09	1.23 ± 0.12	0.94 ± 0.10
11.77	16.9 ± 2.61	6.92 ± 1.08	2.94 ± 0.39	1.95 ± 0.24	1.28 ± 0.14	0.84 ± 0.10	0.75 ± 0.09	0.92 ± 0.12	0.71 ± 0.10
14.82	10.3 ± 2.36	5.22 ± 0.97	2.92 ± 0.36	1.53 ± 0.23	0.94 ± 0.14	0.60 ± 0.10	0.59 ± 0.09	0.69 ± 0.11	0.52 ± 0.10
18.66	10.0 ± 2.20	5.54 ± 0.90	1.81 ± 0.34	1.27 ± 0.23	0.75 ± 0.14	0.44 ± 0.09	0.40 ± 0.09	0.52 ± 0.11	0.36 ± 0.10
23.49	11.1 ± 2.10	5.72 ± 0.86	1.61 ± 0.33	0.95 ± 0.22	0.64 ± 0.14	0.45 ± 0.09	0.37 ± 0.09	0.53 ± 0.11	0.27 ± 0.10
29.57	7.79 ± 2.03	3.87 ± 0.82	0.91 ± 0.32	0.63 ± 0.22	0.38 ± 0.14	0.27 ± 0.09	0.26 ± 0.09	0.51 ± 0.11	0.22 ± 0.10
37.22	7.51 ± 1.99	2.60 ± 0.80	1.01 ± 0.32	0.57 ± 0.22	0.41 ± 0.14	0.23 ± 0.09	0.14 ± 0.09	0.35 ± 0.11	0.21 ± 0.10
46.86	5.49 ± 1.96	2.88 ± 0.79	0.91 ± 0.31	0.69 ± 0.22	0.35 ± 0.14	0.12 ± 0.09	0.05 ± 0.09	0.13 ± 0.11	0.25 ± 0.10
58.99	2.21 ± 1.94	2.37 ± 0.78	0.91 ± 0.31	0.67 ± 0.22	0.33 ± 0.14	0.12 ± 0.09	-0.07 ± 0.09	0.23 ± 0.11	0.05 ± 0.10
74.27	4.96 ± 1.92	1.75 ± 0.77	0.67 ± 0.31	0.60 ± 0.22	0.23 ± 0.14	0.11 ± 0.09	-0.06 ± 0.09	0.30 ± 0.11	0.06 ± 0.10
93.50	5.94 ± 1.92	0.79 ± 0.77	0.44 ± 0.31	0.53 ± 0.22	0.24 ± 0.14	0.23 ± 0.09	0.04 ± 0.09	0.40 ± 0.11	0.12 ± 0.10

^aDivide $\omega(\theta)$ results by 100 to get actual values

Table 3. Measured $\omega(\theta)$ Parameters

I_{median}	N_{gal}	δ^a	δ^b	$\omega(0.5')_{Cor}^c$	$\omega(1')_{Cor}^c$	$\omega(3')_{Cor}^c$	IC Corr.	C_s Corr. ^d
16.46	1443	-0.879 ± 0.058	-0.688 ± 0.087	202 ± 101	137 ± 52.0	56.4 ± 15.6	0.0379	1.167
17.64	3245	-0.807 ± 0.054	-0.739 ± 0.079	80.4 ± 41.2	53.9 ± 19.5	25.0 ± 6.46	0.0151	1.108
18.62	9987	-0.796 ± 0.043	-0.690 ± 0.061	30.1 ± 11.9	22.5 ± 5.70	9.86 ± 2.06	0.0061	1.069
19.61	27246	-0.809 ± 0.034	-0.808 ± 0.041	23.7 ± 4.17	13.6 ± 2.09	5.56 ± 0.83	0.0044	1.046
20.59	62913	-0.783 ± 0.028	-0.739 ± 0.030	13.6 ± 1.75	8.30 ± 0.91	3.55 ± 0.41	0.0027	1.033
21.27	55245	-0.788 ± 0.033	-0.639 ± 0.041	8.91 ± 1.96	6.19 ± 0.99	2.78 ± 0.39	0.0018	1.025
21.77	78082	-0.742 ± 0.029	-0.674 ± 0.034	8.22 ± 1.37	5.26 ± 0.70	2.48 ± 0.39	0.0017	1.022
22.27	106975	-0.627 ± 0.034	-0.475 ± 0.042	5.89 ± 1.39	4.55 ± 0.74	2.44 ± 0.34	0.0014	1.020
22.77	137538	-0.697 ± 0.034	-0.483 ± 0.035	4.05 ± 1.03	4.19 ± 0.55	2.25 ± 0.27	0.0016	1.019

^aSlope for the best fit power law in the range $1' \leq \theta \leq 20'$.

^bSlope for the best fit power law in the range $0.5' \leq \theta \leq 5'$.

^cDivide by 100 to get actual amplitude. Based on a local interpolation to provide a more accurate estimate of the amplitude. The IC and stellar contamination (C_s) corrections have been applied. Corrected $\omega(\theta) = C_s(\omega(\theta)_{obs} + IC)$

^dStellar contamination correction factor, $C_s = N_{Obj}^2 / (N_{Obj} - N_{Star})^2$.

Table 4. Best-fit r_o and ϵ values (1 arcminute scale)

Sample	$N(z)$ Model	r_o (h^{-1} Mpc)	σ_{r_o} at fixed ϵ	ϵ	σ_ϵ^a at fixed r_o	χ_ν^{2b}	Covar. slope ^c	Covar. Intercept ^c	r_o Range ^d	ϵ Range ^d
$I \leq 20$	CFRS	4.70	0.32	-1.50	0.42	0.11	0.768	5.822	3 to 7	-3 to +1
$I \leq 20$	EvLF $\beta = 1$	5.30	0.35	+2.30	0.64	0.29	0.555	4.577	3 to 7	-3 to +4
$I \leq 20$	EvLF $\beta = 1.5$	5.20	0.33	+1.20	0.66	0.30	0.495	4.209	3 to 7	-3 to +4
$I \leq 20$	EvLF $\beta = 2$	5.30	0.36	+0.40	0.57	0.30	0.624	5.060	3 to 7	-3 to +4
$I \leq 23$	CFRS	5.60	0.23	-0.20	0.17	0.24	1.356	5.874	4 to 7	-1.5 to +1
$I \leq 23$	EvLF $\beta = 1$	3.80	0.15	-0.80	0.21	0.39	0.713	4.389	2.7 to 5	-2.5 to +1
$I \leq 23$	EvLF $\beta = 1.5$	3.80	0.15	-1.40	0.18	0.35	0.830	4.954	2.8 to 5.1	-2.7 to 0
$I \leq 23$	EvLF $\beta = 2$	4.10	0.16	-1.70	0.16	0.26	1.025	5.798	3 to 5.2	-2.8 to -0.5
$I \leq 23$	CFRS	5.50 Fixed	...	-0.30	0.75	0.25
$I \leq 23$	EvLF $\beta = 1$	5.50 Fixed	...	+1.30	0.90	2.09
$I \leq 23$	EvLF $\beta = 1.5$	5.50 Fixed	...	+0.50	0.80	2.06
$I \leq 23$	EvLF $\beta = 2$	5.50 Fixed	...	-0.40	0.70	1.83

^aUncertainties in ϵ at fixed r_o are the 1σ values except when r_o is kept fixed. In that case, the errors shown are the 2σ values.

^bThe reduced χ^2 value.

^cThe slope and intercept for the best-fit line to the 1σ χ^2 contour. The line is $r_o = (\text{slope})\epsilon + \text{intercept}$. Values are the average parameters derived from the fits $r_o = f(\epsilon)$ and $\epsilon = f(r_o)$.

^dThe r_o and ϵ range over which the fit to the 1σ χ^2 contour is valid.